Inorganic Chemistry

Article

pubs.acs.org/IC

Cyclams with Ambidentate Methylthiazolyl Pendants for Stable, Inert, and Selective Cu(II) Coordination

Aurora Rodríguez-Rodríguez,[†] Zakaria Halime,[†] Luís M. P. Lima,[‡] Maryline Beyler,[†] David Deniaud,[#] Nicolas Le Poul,[†] Rita Delgado,*[,‡] Carlos Platas-Iglesias,*[,§] Véronique Patinec,[†] and Raphaël Tripier*[,†]

[†]UFR des Sciences et Techniques, Université de Bretagne Occidentale, UMR-CNRS 6521, 6 avenue Victor le Gorgeu, C.S. 93837, 29238 Brest Cedex 3, France

[‡]Instituto de Tecnologia Química e Biológica António Xavier, Universidade Nova de Lisboa, Av. da República, 2780-157 Oeiras, Portugal

[#]UFR Sciences et Techniques, Université de Nantes, UMR-CNRS 6230, 2, rue de la Houssinière, BP 92208, 44322 Nantes Cedex 3, France

[§]Grupo QUICOOR, Centro de Investigaciones Científicas Avanzadas (CICA) and Departamento de Química Fundamental, Facultade de Ciencias, Universidade da Coruña, Campus da Zapateira-Rúa da Fraga 10, 15008 A Coruña, Spain

Supporting Information

ABSTRACT: Aiming to develop new copper chelates for application in nuclear medicine we report two new chelators, **te1th** and **te2th**, based on a cyclam backbone mono-*N*- or di-N_1,N_8-functionalized by methylthiazolyl arms. The acid−base properties of both ligands were investigated as well as their coordination chemistry, especially with Cu^{2+}, when possible in aqueous solution and in the solid state. Single-crystal X-ray diffraction structures of complexes were determined. Stability constants of the copper(II) and zinc(II) complexes showed that the complexes of both ligands with Cu^{2+} are thermodynamically very stable, and they exhibit an important selectivity for Cu^{2+} over Zn^{2+}. The kinetic inertness in acidic medium of both copper(II) complexes was evaluated revealing a quite good resistance to dissociation (the half-life times of complexes with **te1th** and **te2th** are 50.8 and 5.8 min, respectively, in 5 M HCl and 30 °C). The coordination geometry of the metal center in the complexes was established in aqueous solution based on UV−visible, electron paramagnetic resonance (EPR) spectroscopy, DFT studies, and NMR by using the zinc(II) complex analogues. The [Cu(**te1th**)]$^{2+}$ and [Cu(**te2th**)]$^{2+}$ complexes adopt *trans*-I and *trans*-III configurations both in the solid state and in solution, while the [Zn(**te2th**)]$^{2+}$ complex crystallizes as the *cis*-V isomer but exists in solution as a mixture of *trans*-III and *cis*-V forms. Cyclic voltammetry experiments in acetonitrile point to a relatively easy reduction of [Cu(**te2th**)]$^{2+}$ in acetonitrile solution (E_{pc} = −0.41 V vs NHE), but the reduced complex does not undergo dissociation in the time scale of our electrochemical experiments. The results obtained in these studies revealed that despite the limited solubility of its copper(II) chelate, **te2th** is an attractive chelator for Cu^{2+} that provides a fast complexation process while forming a complex with a rather high thermodynamic stability and kinetic inertness with respect to dissociation even upon electrochemical reduction.

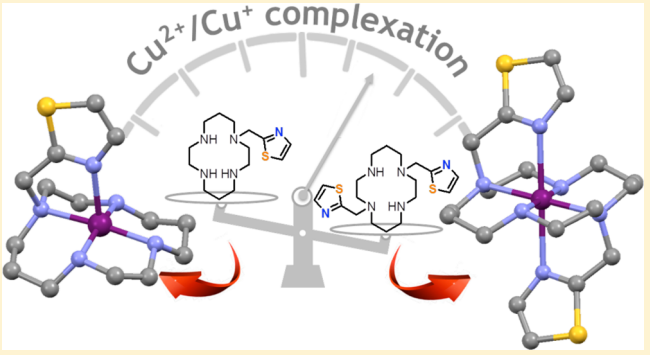

INTRODUCTION

Positron emission tomography (PET) is a molecular imaging technique for diagnosis and monitoring of disease that has experienced a growing development in the last 15 years. This success is partly related to the current easier access to radionuclides from reactors or generators. Furthermore, PET is a non-invasive technique that only requires a picomolar quantity of the injected active radiopharmaceutical, while providing high resolution images at the millimeter scale. ^{18}F ($t_{1/2}$ = 110 min, E = 0.64 MeV) in the form of ^{18}F-FDG (2-fluoro-2-deoxyglucose) is currently the most used radiopharmaceutical in clinical practice for moderately long *in vivo* investigation.[1] Nevertheless, monitoring biological processes with slower pharmacokinetics requires radionuclides with longer half-life times such as ^{64}Cu, which has a 12.7 h half-life time and low positron energy (E = 0.65 MeV). Thus, $^{64}Cu^{2+}$-based radiopharmaceuticals are currently the subject of intense research efforts.[2]

$^{64}Cu^{2+}$-based probes for PET imaging are usually bifunctional chelating agents (BCAs) that contain a chelating unit to sequester the radioactive metal ion linked to a biological vector such as a peptide or an antibody.[3] Obviously the couple chelator-radionuclide has to be adequately matched to avoid

Received: August 5, 2015

DOI: 10.1021/acs.inorgchem.5b01779
Inorg. Chem. XXXX, XXX, XXX−XXX

Chart 1. Structures of Ligands Discussed in This Work

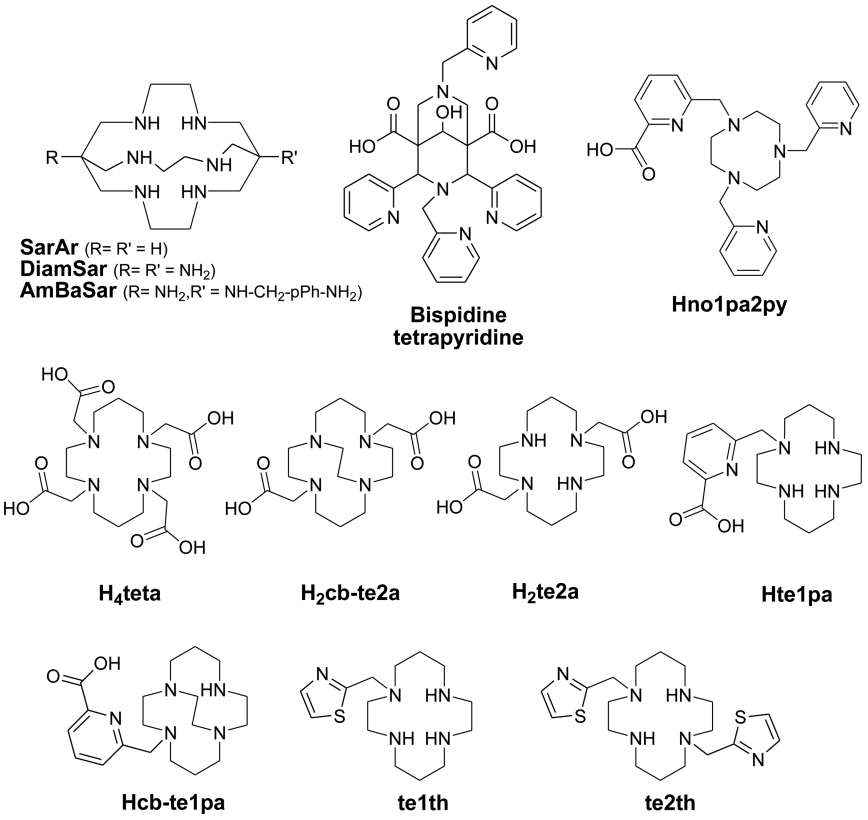

transchelation or transmetalation in biological media. Indeed, the radiopharmaceutical has to fulfill different important requirements in terms of physicochemical and biochemical properties for a potential clinical use:[4] (i) fast complexation of the radioelement under mild conditions to optimize the radionuclide action, (ii) high metal binding affinity with high selectivity in the presence of other *in vivo* competitive metal ions such as Zn^{2+}, (iii) high kinetic inertness to avoid the release of ^{64}Cu(II) from the ligand, and (iv) inertness toward demetalation upon Cu(II) → Cu(I) reduction.

Different researchers have studied the physicochemical properties of chelator families with the non-radioisotopes Cu(II)/Cu(I) couple as potential chelators for PET imaging.[5] Due to the borderline hardness of the Cu^{2+} cation, ligands containing nitrogen atoms such as cyclic polyamines,[5] sarcophagines (Sar ligands)[6] or bispidines[7] have demonstrated their ability to form chelates of interest. Among the polyazacycloalkane family, copper(II) complexes of $dota^{4-}$ and $teta^{4-}$ derivatives have shown better thermodynamic stability than those of the corresponding non-macrocyclic analogues such as $dtpa^{5-}$, but nevertheless a lack of kinetic inertness.[5] Constrained tetraazamacrocycles such as the cross-bridged $cb\text{-}te2a^{2-}$ (Chart 1) lock up the metallic cation giving complexes with both high thermodynamic stabilities and high kinetic inertness, but unfortunately they show slow complexation kinetics.[8] The following order of chelators for *in vivo* radiocopper stability has been proposed: $dota^{4-}$, $teta^{4-}$ < $cb\text{-}te2a^{2-}$ ≪ Sar-Ar ∼ AmBaSar,[9] which suggests that N6 constrained chelators are good candidates for PET imaging applications. Another strategy developed for improving the *in vivo* ^{64}Cu stability relied on the incorporation of the bidentate picolinate group in different macrocyclic platforms such as cyclam ($te1pa^{-}$),[10] cross-bridged cyclam ($cb\text{-}te1pa^{-}$),[11] and triazacyclononane ($no1pa2py^{-}$).[12] The bidentate nature of the picolinate group used as pendant arm was found to result in a beneficial improvement of the rate of complex formation while keeping good thermodynamic stability and kinetic inertness.

The *in vivo* bioreduction of Cu(II) to Cu(I) has already been proposed as a probable cause of *in vivo* radiocopper loss in ^{64}Cu-based radiopharmaceuticals.[13] The higher lability and lower thermodynamic stability of the Cu(I) complex in comparison with the Cu(II) one might be sufficient to cause complex dissociation. Indeed, the dissociation of the complex upon reduction of Cu(II) to Cu(I) was proved to be a key step in the mechanism of hypoxia by copper radiopharmaceuticals.[14,15] With this in mind, we envisaged that ligands incorporating ambidentate coordinating groups with both nitrogen and sulfur donor atoms may potentially stabilize the two oxidation states of copper (Cu^{2+} and Cu^{+}) by changing the nature of the donor atom depending on the oxidation state of the metal.[16] To test this, we appended the new ambidentate nitrogen/sulfur arms on the cyclam skeleton, which forms positively charged complexes to offer other behavior for in vivo applications.

In this work, we describe the synthesis of two new copper chelators based on a cyclam platform functionalized with one or two methylthiazolyl pendant arms (**te1th** and **te2th**, respectively), expecting that Cu^{2+} and Cu^{+} ions might be coordinated respectively by the harder nitrogen and the softer sulfur donor atoms of the arms. The structures of the Cu(II) and Zn(II) complexes with the two ligands were studied both in the solid state and in solution. The thermodynamic stabilities of the complexes have been investigated using potentiometric or spectrophotometric titrations, while complexation and

DOI: 10.1021/acs.inorgchem.5b01779
Inorg. Chem. XXXX, XXX, XXX−XXX

dissociation kinetics were assessed using spectrophotometric techniques. The electrochemical and chemical reductions of the Cu(II) complexes were also investigated. All along the discussion, the properties of the two chelators are compared with related ligands having similar structures.

RESULTS AND DISCUSSION

Ligands Synthesis. The key reactant for the synthesis of both ligands is 2-(bromomethyl)-thiazole (**1**), which has been obtained by bromination of the thiazol-2-ylmethanol precursor.[17] The synthesis of **te1th** was achieved in three steps with a good overall yield (57%) following the phosphorylcyclam method (Scheme 1).[18] Thus, triprotection of cyclam with a phosphoryl group was followed by alkylation of the secondary free amine with **1** and deprotection in acidic conditions. The bromomethyl derivative **1** was also reactive enough to allow dialkylation of bisformyl cyclam (**4**), which was obtained by reaction of cyclam and aqueous formaldehyde.[19] Hydrolysis of the diammonium salt **5** in basic conditions gave 1,8-di(methylthiazolyl)cyclam (**te2th**) with an overall yield of 57% for the three steps (Scheme 1). All compounds were fully characterized, and NMR and MS spectra are presented in Figures S1−S8.

Scheme 1. Ligands Synthesis and Atom Labeling[a]

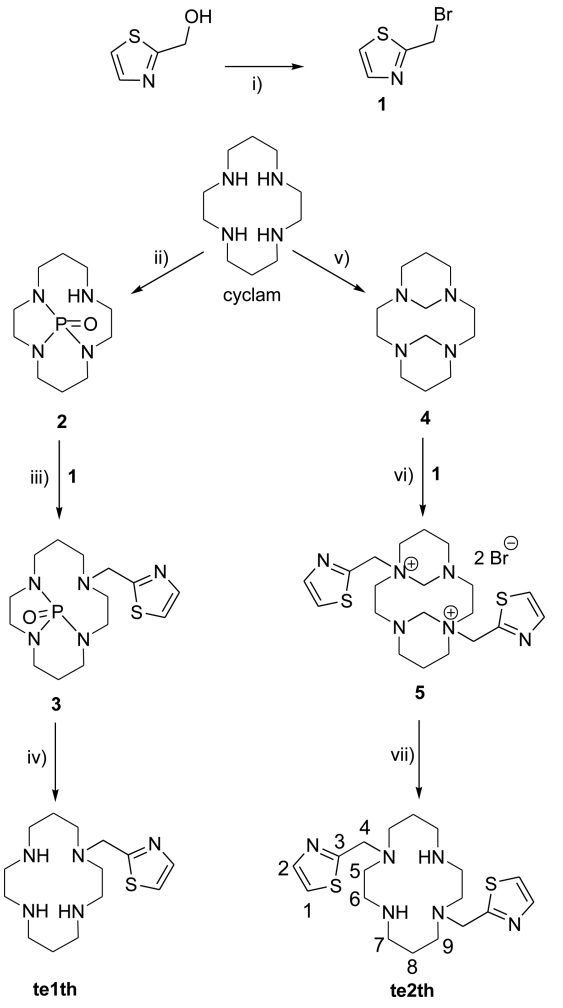

[a]Reagents and conditions: (i) PBr_3, CH_2Cl_2, reflux, 5 h, quantitative; (ii) $P(NMe_2)_3$, toluene, reflux; CCl_4; 4 M NaOH, 75%; (iii) **1**, K_2CO_3, CH_3CN, RT, 48 h, 85%; (iv) 3 M HCl, RT, 12 h, 89%; (v) HCOH, H_2O, RT, 4 h, quantitative; (vi) **1**, CH_3CN, RT, 96 h, 68%; (vii) 4 M NaOH, RT, 12 h, 84%.

The molecular structures of the two ligands were confirmed by single-crystal X-ray diffraction analyses. ORTEP views, crystallographic data of the structures, and discussion are given in Figure S9 and Table S1.

Synthesis and Characterization of the Copper(II) and Zinc(II) Complexes. The synthesis of the complexes of **te1th** was carried out in water using $M(ClO_4)_2{\cdot}6H_2O$ (M = Cu, Zn) at pH 6−7. The complexes were isolated as purple $[Cu(\mathbf{te1th})](ClO_4)_2$ and white $[Zn(\mathbf{te1th})](ClO_4)_2$ perchlorate salts in 97% and 85% yields, respectively. Single crystals were isolated by slow evaporation of aqueous solutions of both complexes, but only those of the Cu(II) analogues were suitable for single-crystal X-ray diffraction studies. Crystals of the complex are composed of the cationic entity $[Cu(\mathbf{te1th})]^{2+}$ and two perchlorate anions. A view of the structure of the complex cation is shown in Figure 1, while bond distances of the metal coordination environment are compiled in Tables 1 and S2. The metal ion is directly bound to the five nitrogen donor atoms of the ligand. Three NH groups of the cyclam unit and the pendant arm are pointing to the same side of the cyclam unit, which results in a *trans*-I configuration.[20] This configuration is usually favorable over the *trans*-III configuration in five-coordinate Cu(II) complexes of cyclam-based ligands.[21] In the *trans*-III configuration two adjacent N-R groups of the macrocycle (R = H or the alkyl group) are directed toward one side of the cyclam plane, and the other two point to the opposite side of the plane. The Cu−N distances involving donor atoms of the cyclam unit (1.97−2.07 Å) are close to those observed for different five-coordinate copper(II) complexes of cyclam derivatives containing a N5 donor set.[22] The distance between Cu and the nitrogen donor atom of the pendant arm [2.252(7) Å] is clearly longer than the remaining Cu−N bond distances. The coordination polyhedron around the Cu atom can be best described as distorted square pyramidal, with the four donor atoms of the macrocycle describing the basal plane and the nitrogen atom of the thiazol group at the apical position. The metal ion is placed 0.156 Å above the least-squares plane defined by the donor atoms of the cyclam fragment. The *trans* angles are relatively close to the

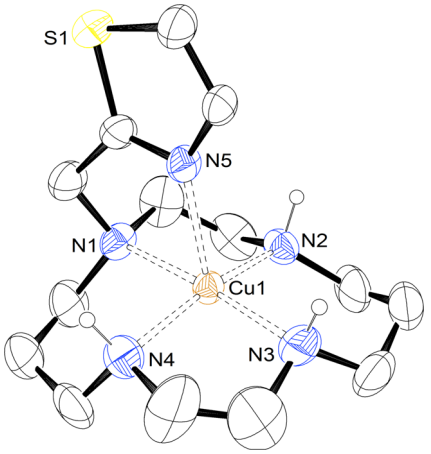

Figure 1. View of the crystal structure of $[Cu(\mathbf{te1th})](ClO_4)_2$. Hydrogen atoms linked to carbon atoms and anions have been omitted for simplicity. The ORTEP plot is at the 30% probability level.

DOI: 10.1021/acs.inorgchem.5b01779
Inorg. Chem. XXXX, XXX, XXX−XXX

Table 1. Bond Lengths (Å) of the Metal Coordination Environments Observed in the X-ray Structures of $[Cu(te1th)]^{2+}$, $[Cu(te2th)]^{2+}$, and $[Zn(te2th)]^{2+}$ Complexes

$[Cu(te1th)]^{2+}$		$[Cu(te2th)]^{2+}$		$[Zn(te2th)]^{2+}$	
Cu1−N1	2.070(7)	Cu1−N1	2.0853(15)	Zn1−N1	2.202(3)
Cu1−N2	1.971(8)	Cu1−N2	2.0032(15)	Zn1−N2	2.157(2)
Cu1−N3	2.011(9)	Cu1−N3	2.4575(16)	Zn1−N3	2.203(2)
Cu1−N4	2.008(8)			Zn1−N4	2.159(3)
Cu1−N5	2.252(7)			Zn1−N5	2.220(3)
				Zn1−N6	2.147(3)

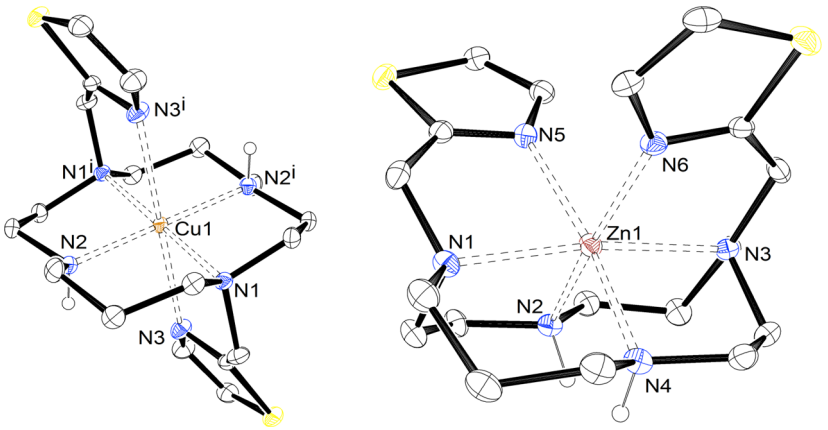

Figure 2. Views of the crystal structures of $[Cu(te2th)](ClO_4)_2$ (left) and $[Zn(te2th)](ClO_4)_2{\cdot}H_2O$ (right). Hydrogen atoms linked to carbon atoms, anions, and water molecules have been omitted for simplicity. The ORTEP plots are at the 30% probability level.

ideal value of 180° [N1−Cu−N3 = 175.4(4)° and N2−Cu−N4 = 165.6(3)°], while the angles involving the apical donor and donor atoms delineating the basal plane fall within the range of 79.9−103.7°. The square pyramidal coordination around the metal center is confirmed by performing continuous shape measures with the assistance of the SHAPE program,[23,24] which provides shape measures for square pyramidal and trigonal bipyramidal coordination of 1.29 and 4.85, respectively (the shape measure S(A) = 0 for a structure fully coincident in shape with the reference polyhedron, and the maximum allowed value of S(A) is 100).

Complexes of **te2th** were synthesized by reacting equimolar amounts of the ligand and $M(ClO_4)_2{\cdot}6H_2O$ (M = Cu or Zn) in a refluxing acetonitrile/methanol mixture. The $[Cu(te2th)](ClO_4)_2$ and $[Zn(te2th)](ClO_4)_2$ complexes were isolated respectively as purple and white solids in 89% and 74% yield. Single crystals of $[Cu(te2th)](ClO_4)_2$ and $[Zn(te2th)](ClO_4)_2{\cdot}H_2O$ were obtained by slow evaporation of the solvent mixture. ORTEP views of the structures of the complex cations are shown in Figure 2. The $[Cu(te2th)]^{2+}$ complex presents a crystallographically imposed C_i symmetry, with the metal coordination environment being best described as tetragonally elongated octahedral, which is typical of copper(II) complexes with Jahn−Teller distortion. Indeed, the Cu−N distances involving the donor atoms of the pendant arms (Cu1−N3 = 2.4575(16) Å) are considerably longer than the Cu1−N1 and Cu1−N2 distances (Tables 1 and S2). The macrocycle in the complex adopts a *trans*-III configuration, with one of the pendant arm and a N−H group pointing to one side of the macrocyclic unit and the second pendant arm and another N−H group pointing to the opposite side. Similar *trans*-III configurations with elongated octahedral coordination have been previously observed for cyclam-based ligands containing two coordinating pendant arms.[25] However, in some cases, cyclam derivatives containing potentially coordinating arms in *trans* positions form five-coordinate complexes with *trans*-I configuration.[26]

In contrast, the two pendant arms point to the same side of the cyclam unit in the $[Zn(te2th)]^{2+}$ complex, which adopts an unusual *cis*-V configuration (Figure 2). The metal coordination environment in $[Zn(te2th)]^{2+}$ is distorted octahedral, with *trans* angles in the range 168.7−171.4°, and *cis* angles varying from ca. 75.5 to 106.9°, reflecting a significant distortion of the coordination polyhedron from the regular octahedral geometry.

Acid−Base Properties of the Ligands and Thermodynamic Stability of Their Complexes with Cu^{2+} and Zn^{2+} Cations. The protonation constants of the ligands were determined by potentiometric titrations in aqueous solutions (Table 2). Speciation diagrams of the protonated species of the ligands are presented in Figure S10. Due to the very low basicity of the thiazolyl moieties, both compounds display only two protonation equilibria that must correspond to the

Table 2. Overall (β_i^H) and Stepwise (K_i^H) Protonation Constants, in log Units, of te1th and te2th, at 25.0 °C in 0.10 M KNO_3

equilibrium reaction[a]	te1th[b]	te2th[b]
	log β_i^H	
$L + H^+ \rightleftarrows HL$	10.74(1)	10.09(1)
$L + 2H^+ \rightleftarrows H_2L$	20.05(3)	18.51(1)
	log K_i^H	
$L + H^+ \rightleftarrows HL$	10.74(1)	10.09(1)
$HL + H^+ \rightleftarrows H_2L$	9.31(3)	8.42(1)

[a]L denotes the ligand in general; charges are omitted for simplicity. [b]Values in parentheses are standard deviations in the last significant figures.

DOI: 10.1021/acs.inorgchem.5b01779
Inorg. Chem. XXXX, XXX, XXX−XXX

protonation of opposite amines of each macrocycle. The overall basicity is slightly higher for **te1th** than for **te2th**, with both compounds being moderately basic.

The thermodynamic stability constants of the copper(II) complexes were also determined by potentiometric titrations in aqueous solutions. Additionally, the stability constants of the complexes of Zn^{2+} were likewise determined, as this ion can act as a competitor for Cu^{2+} *in vivo*. The stepwise ($\log K_{MHhL}$) and overall ($\log \beta_{MHhL}$) stability constants determined are given in Table 3, together with literature values for H_4teta, while

Table 3. Overall (β_{MH_hL}) and Stepwise (K_{MH_hL}) Stability Constants, in log Units, for Complexes of te1th, te2th, and H_4teta Ligands with Cu^{2+} and Zn^{2+} Cations, at 25.0 °C in I = 0.10 M KNO_3

equilibrium reaction[a]	te1th[b]	te2th[b]	H_4teta[c]
	log β_{MH_hL}		
$Cu^{2+} + L \rightleftarrows CuL$	21.56(2)	19.9(2)	21.07
$Cu^{2+} + L \rightleftarrows CuLH_{-1} + H^+$	10.4 (1)		
$Zn^{2+} + L \rightleftarrows ZnL$	15.38(2)	14.41(1)	17.48
$Zn^{2+} + H^+ + L \rightleftarrows ZnHL$		17.69(6)	21.64
$Zn^{2+} + L \rightleftarrows ZnLH_{-1} + H^+$	6.24(5)		6.68
	log K_{MH_hL}		
$Cu^{2+} + L \rightleftarrows CuL$	21.56(2)	19.9(2)	21.07
$CuLOH + H^+ \rightleftarrows CuL$	11.2 (1)		
$Zn^{2+} + L \rightleftarrows ZnL$	15.38(2)	14.41(1)	17.48
$ZnL + H^+ \rightleftarrows ZnHL$		3.28(6)	4.16
$ZnLOH + H^+ \rightleftarrows ZnL$	9.14(4)		10.8

[a]L denotes the ligand in general; charges of ligand and complex species are omitted for simplicity. [b]Values in parentheses are standard deviations in the last significant figures. [c]The complete system includes the MHL and MH_2L species for Cu^{2+} and MH_2L for Zn^{2+}, see ref 27, Table 3.

speciation diagrams of both ligands in the presence of the cations are presented in Figures S11 and S12. The complexation of Zn^{2+} was rather slow for both **te1th** and **te2th** in the acidic pH range; thus, out-of-cell titrations were performed in the range of pH 3−5 in order to complement the usual in-cell titrations. In the case of Cu^{2+}, the study was rendered difficult for both ligands because of the high complexation extent occurring even at a very low pH which prevents a direct determination of the stability constants. To overcome this problem, out-of-cell competition titrations were performed using H_4edta as the competitor ligand.

A more accurate assessment of the complexation efficiency of the ligands can be made by determining their pM values ($-\log [M]_{free}$), which take into account the different basicity of the ligands and the full set of stability constants for each system. The pM values determined at physiological pH for the two metal ions from the constants of Tables 2 and 3 are given in Table 4. As expected, the stability constants (and the corresponding pM values) are very high for both complexes of **te1th** and **te2th** with Cu^{2+}, while they significantly decrease for the Zn^{2+} analogues. Importantly, these values demonstrate that while **te1th** and **te2th** have a high and approximately equivalent efficiency for Cu^{2+} complexation, they also show a high selectivity for Cu^{2+} over Zn^{2+}. Compared to the well-known H_4teta ligand with a similar structure, both studied ligands exhibit a higher affinity for Cu^{2+} while preserving a good

Table 4. Calculated pM Values for the Complexes of te1th, te2th, and H_4teta Compounds

	te1th[a]	te2th[a]	H_4teta[b]
Cu^{2+}	16.30	16.17	14.20
Zn^{2+}	10.13	10.66	10.61

[a]Values calculated at pH 7.4 for 100% excess of ligand with $[M^{2+}]_{tot} = 1.0 \times 10^{-5}$ M, based on the reported stability constants. [b]Taken from ref 27, Table 4.

selectivity over Zn^{2+} ions, thus proving to be thermodynamically suitable for an efficient Cu^{2+} complexation.

Structures of the Zinc(II) and Copper(II) Complexes in Solution. The zinc(II) complexes were studied in solution by NMR experiments, while, because of its paramagnetic character, the Cu^{2+} analogues were investigated by UV−vis and EPR spectroscopies. All 1D and 2D NMR spectra are presented in Figures S13−S19. The ^{1}H and ^{13}C NMR spectra of the $[Zn(\mathbf{te1th})]^{2+}$ complex were recorded in D_2O solution at neutral pH and point to the presence of a major species in solution. The ^{13}C NMR spectrum presents 14 signals, as expected for a complex with a C_1 symmetry. The ^{1}H spectrum shows the expected signals of the thiazole group at 8.04 and 7.94 ppm, and an AB spin system for the methylene protons of the pendant arm with signals at 4.30 and 4.58 ppm (^2J = 17.6 Hz). However, the complexity of the spectra due to the low symmetry of the complex prevented their complete assignment. DFT calculations at the TPSSh/TZVP level provide three minimum energy conformations corresponding to the *trans*-I, *trans*-III, and *cis*-V isomers, with relative Gibbs free energies of 0.0, 9.8, and 10.8 kJ mol^{-1}, respectively (Figure S20). These results suggest that the $[Zn(\mathbf{te1th})]^{2+}$ complex adopts a *trans*-I configuration in solution similar to that observed in the solid state for the Cu^{2+} analogue.

The NMR spectra of the $[Zn(\mathbf{te2th})]^{2+}$ complex recorded in CD_3CN solution were considerably more informative. The ^{1}H NMR spectrum (Figure 3) displays two sets of signals with

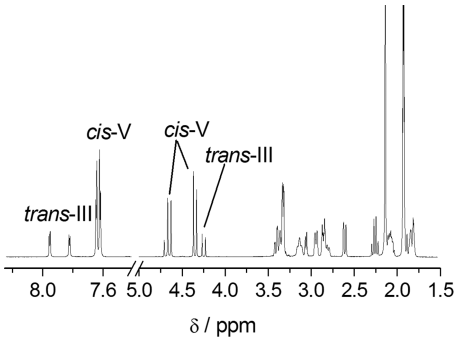

Figure 3. ^{1}H NMR spectrum (500 MHz) of $[Zn(\mathbf{te2th})](ClO_4)_2$ recorded in CD_3CN solution at 25 °C. The solvent signals have been truncated for better visualization.

different intensity, which points to the presence of two complex species in solution. This is confirmed by the ^{13}C NMR spectrum, which shows two sets of signals each one consisting of nine resonances. The ^{1}H and ^{13}C NMR signals of the major species (ca. 78%) could be completely assigned with the aid of homonuclear ^{1}H−^{1}H COSY and heteronuclear ^{1}H−^{13}C HMQC and HMBC spectra, while in the case of the minor species (ca. 22%) only the ^{13}C NMR spectrum could be completely attributed (Table 5). According to previous

DOI: 10.1021/acs.inorgchem.5b01779
Inorg. Chem. XXXX, XXX, XXX−XXX

Table 5. ^{1}H and ^{13}C NMR Data for the *cis*-V and *trans*-III Isomers of $[Zn(te2th)]^{2+}$ in CD_3CN Solution at 25 °C

	cis-V			*trans*-III
H1	7.64	C1	124.3	124.2
H2	7.63	C2	139.9	141.3
$H4_{ax}$	4.36	C3	171.3	172.5
$H4_{eq}$	4.66	C4	61.9	57.1
$H5_{ax}$	3.41	C5	56.0	61.7
$H5_{eq}$	2.61	C6	47.0	46.2
$H6_{ax}$	1.91	C7	50.8	49.8
$H6_{eq}$	2.86	C8	25.9	26.2
$H7_{ax}$	2.25	C9	61.9	60.5
$H7_{eq}$	2.95			
$H8_{ax}$	2.10			
$H8_{eq}$	1.82			
$H9_{ax}$	3.33			
$H9_{eq}$	3.33			

studies,[28] the attribution of the axial and equatorial protons of the cyclam fragment was achieved by analyzing the ^{2}J and ^{3}J coupling patterns of the different signals.

Indeed, the axial protons provide two strong couplings, the $^{2}J_{ax\text{-}eq}$ coupling (~16 Hz) and the $^{3}J_{ax\text{-}ax}$ coupling (~14 Hz), while equatorial protons give only one strong coupling ($^{2}J_{eq\text{-}ax}$). For instance the signal at 2.61 ppm (Figure 3) is observed as a pseudo-doublet, and therefore corresponds to an equatorial proton, while the signal at 2.25 ppm is assigned to axial protons, as it presents two $^{1}H-^{1}H$ couplings of similar magnitude.

To assist the assignment of the isomers of $[Zn(\mathbf{te2th})]^{2+}$ present in solution we performed DFT calculations at the TPSSh/TZVP level (Figure S21).[29] The NMR spectra indicate that the two forms present in solution possess C_2, C_i or C_s symmetries, which is only compatible with the *cis*-V, *trans*-I, and *trans*-III isomers.[20] However, the *trans*-I isomer can be ruled out because of the steric hindrance created by the simultaneous coordination of the two pendant arms on the same side of the cyclam unit. Our DFT calculations performed in acetonitrile solution indeed provide the *cis*-V and *trans*-III isomers as minimum energy conformations with a relative Gibbs free energy that favors the *trans*-III form by only 1.9 kJ mol^{-1}. Given this small relative free energy, it is likely that these two isomers present significant populations in solution. The optimized structure obtained for the *cis*-V isomer is in good agreement with the X-ray structure described above. To aid the assignment of the experimental spectra DFT was used to calculate the ^{13}C NMR shifts of the two isomers (see Computational Details below). The experimental ^{13}C NMR shifts observed for the two isomers present in solution are relatively similar (Table 5), differing by <1.2 ppm for all carbon nuclei except C4 ($\Delta\delta$ = 4.8 ppm) and C5 ($\Delta\delta$ = 5.7 ppm). The ^{13}C NMR chemical shifts obtained with DFT for the *cis*-V and *trans*-III isomers are also very similar for all carbon atoms except C5, for which chemical shifts of 53.6 and 61.7 ppm are predicted for the *cis*-V and *trans*-III isomers. Considering the corresponding experimental values (56.0 and 61.7 ppm), we tentatively assign the major isomer present in solution to the *cis*-V isomer and the minor isomer to the *trans*-III isomer.

The structure of the $[Cu(\mathbf{te1th})]^{2+}$ and $[Cu(\mathbf{te2th})]^{2+}$ complexes in solution was investigated by EPR spectroscopy. The experimental X-band EPR spectra of the complexes are presented in Figure 4 together with the spectra simulated with the parameters given in Table 6.[30] Both spectra could be

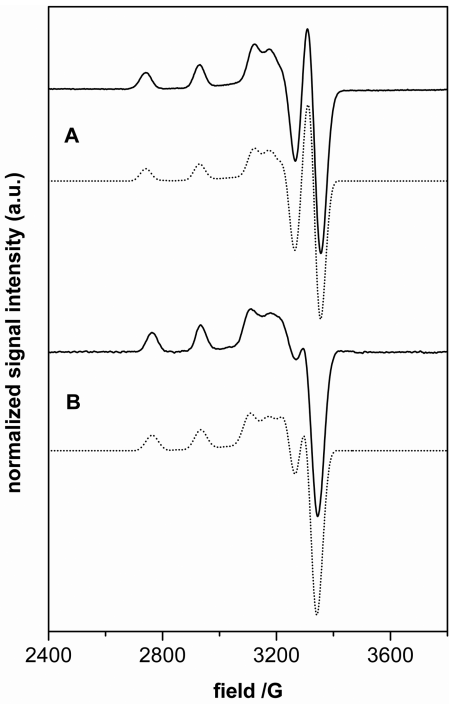

Figure 4. Experimental (full lines) and simulated (dotted lines) X-band EPR spectra of the $[Cu(\mathbf{te1th})]^{2+}$ (A) and $[Cu(\mathbf{te2th})]^{2+}$ (B) complexes recorded in frozen aqueous solution.

simulated assuming the presence of a single paramagnetic species in solution. The spectra are typical of tetragonal complexes with a $d_{x^2-y^2}$ ground state ($g_z > g_x, g_y > g_e$), which points to square planar, square pyramidal or octahedral geometries with elongation of the axial bonds.

The EPR parameters of the copper(II) complexes were further analyzed by calculating the *g*- and *A*-tensors using DFT computations. Recent computational studies demonstrated that the calculation of accurate EPR parameters is a difficult task, the results depend critically upon the method employed, in particular on the functional used.[31] It was found that the accuracy of the calculated *g* values improves considerably upon increasing the amount of exact exchange.[29,31] Thus, the EPR parameters of $[Cu(\mathbf{te1th})]^{2+}$ and $[Cu(\mathbf{te2th})]^{2+}$ complexes were calculated using the TPSS0 functional, a 25% exchange version of TPSSh (10% exchange). The results are listed in Table 6.

Geometry optimizations of the $[Cu(\mathbf{te1th})]^{2+}$ complex performed at the TPSSh/TZVP level in aqueous solution provide the minimum energy geometries corresponding to the *trans*-I, *trans*-III, and *cis*-V isomers (Figure S22). The structure calculated for the *trans*-I configuration are in a good agreement with the experimental X-ray structure described above. The relative Gibbs free energies calculated for the *trans*-I and *trans*-III isomers favor the first by only 0.80 kJ mol^{-1}, while the *cis*-V form possesses a much higher energy, and thus likely plays no role. This is confirmed by the EPR parameters calculated for the *cis*-V isomer, which differ significantly from the experimental values. More specifically, the experimental values obtained for g_x and g_y are rather similar, while for the *cis*-V form our calculations provide a *g*-tensor such as $g_x < g_y$. Furthermore, the *cis*-V form is characterized by lower A_z and higher A_x and A_y values with respect to the experiment. The *g*- and *A*-tensors calculated for the *trans*-I and *trans*-III isomers of $[Cu(\mathbf{te1th})]^{2+}$

DOI: 10.1021/acs.inorgchem.5b01779
Inorg. Chem. XXXX, XXX, XXX−XXX

Table 6. Experimental EPR Parameters and Vis Data Obtained for the $[Cu(te1th)]^{2+}$ and $[Cu(te2th)]^{2+}$ Complexes and Relative Energies of the Different Isomers and EPR Parameters Calculated Using DFT

isomer		λ_{max} (ε)[a]	ΔG^0 [kJ mol^{-1}]	g_x	g_y	g_z	A_x[b]	A_y[b]	A_z[b]
				$[Cu(te1th)]^{2+}$					
	exp	538 (101)		2.04	2.06	2.20	21	24	193
trans-I	calcd[c]		0.00	2.03	2.07	2.15	34	36[d]	196
trans-III	calcd[c]		0.80	2.05	2.05	2.15	0.7	4.7[d]	207[d]
cis-V	calcd[c]		12.2	2.01	2.12	2.14	84[d]	89	137[d]
				$[Cu(te2th)]^{2+}$					
	exp	550 (146)		2.04	2.06	2.20	10	29	180
trans-III	calcd[c]		0.00	2.04	2.06	2.16	11[d]	33	196
cis-V	calcd[c]		32.6	2.01	2.13	2.17	71[d]	95	129[d]

[a] λ_{max} in nm; ε in M^{-1} cm^{-1}. [b] Values of $A_i \times 10^4$ cm^{-1}. [c] Relative energies calculated using the TPSSh functional, and EPR parameters calculated using the TPSS0 functional. [d] Calculated as negative quantities.

are very similar, and therefore it is likely that these two species cannot be distinguished from their EPR spectra. Given the small energy differences between the two isomers it is therefore probable that the *trans*-I and *trans*-III isomers are both present in solution, the overall population being likely dominated by the *trans*-I isomer observed in the X-ray structure described above.

The *trans*-I configuration can be ruled out in the case of $[Cu(te2th)]^{2+}$ due to the steric hindrance generated by the two pendant arms oriented to the same side of the macrocyclic moiety (Figure S23). The EPR parameters calculated for the *trans*-III form is in a good agreement with the experimental data, while the *cis*-V isomer gives rather different calculated *g*- and *A*-tensors. Thus, we conclude that $[Cu(te2th)]^{2+}$ is present in solution as the *trans*-III isomer, which is also in line with the relative energies obtained by DFT calculations (Table 6).

Formation and Dissociation Kinetics of Copper(II) Complexes. The time course of the copper(II) complexation with **te1th** and **te2th** was monitored by measuring the increase in the absorbance of the d−d transition of each complex at pH 5.6 in acetate buffer at RT. Plots of the % of complex formation in function of time (Figure S24) indicate that the complexation of Cu(II) by **te1th** is complete within few seconds, while less than 200 s are necessary to completely form the copper(II) chelate of **tet2th**.

The kinetic inertness of the metal complexes has been evaluated by monitoring the dissociation in acidic medium (Figure S25−S27), which is considered as a relevant test to assess and compare the inertness of metal chelates in competitive media.[32,33] The dissociation of the copper(II) complexes of **te1th** and **te2th** was monitored under pseudo-first-order conditions in aqueous solution by measuring the decrease of the d−d transition band in the visible spectroscopic range. Half-life times were determined in 5 M HCl acidic medium at 30 and 50 °C for comparison with literature data, and results are presented in Table 7. These data show that the $[Cu(te1th)]^{2+}$ complex is very inert with respect to acid dissociation with a half-life time of the same order as that of $[Cu(teta)]^{2-}$, while $[Cu(te2th)]^{2+}$ is considerably more labile. The results for the studied complexes are in line with previous experiments showing that complexes of *N*-substituted cyclam derivatives are generally more labile than complexes with more secondary amino groups,[34] even if that is not verified in comparison with H_4teta probably due to the different nature of the pendant arms.

Table 7. Half-Life Times Determined for the Copper(II) Complexes of te1th and te2th, and Literature Complexes for Comparison

	te1th	te2th	H_4teta	H_2te2a
5 M HCl, 30 °C		50.8 min	3.5 d[a]	
5 M HCl, 50 °C	3.4 h	5.8 min	3.2 h;[a] 4.1 h[b]	92.6 h[b]

[a] From ref 13. [b] From ref 36.

Additionally, the inertness of the $[Cu(te1th)]^{2+}$ and $[Cu(te2th)]^{2+}$ complexes was also tested by challenging with a high excess of H_4edta as competitor ligand, in solutions at pH 7.4 and 37 °C. These tests showed that the two complexes are rather equally inert in such competitive media, as both showed insignificant transchelation after 1 week. This proves the very good resistance of both complexes to transchelation, considering that many copper(II) complexes show significant levels of transchelation with H_4edta after just a few hours.[35]

Electrochemistry of the Cu^{2+} Complexes. Reduction of Cu(II) into Cu(I) followed by demetalation is one of the possible pathways for the dissociation observed in biological medium (threshold of −0.4 V for typical bioreductors) for some ^{64}Cu macrocyclic complexes.[5b,36] Studying the cyclic voltammetry (CV) of Cu(II) complexes gives information about their behavior under reductive conditions at the electrode scale in terms of electrochemical reversibility of the Cu(II)/Cu(I) system. Thus, CV studies were performed at a vitreous carbon working electrode in CH_3CN/NBu_4PF_6 0.1 M because of the poor solubility of $[Cu(te2th)](ClO_4)_2$ in water (see Figure S28), which renders results unexploitable. In order to be consistent with voltammograms shown in Figure 5, the potential values E_{pc} and E_{pa} in the following discussion are given using Fc/Fc^+ as the reference redox couple.

For $[Cu(te1th)]^{2+}$, a reduction peak was detected at E_{pc} = −1.29 V (vs Fc). On the backscan, two oxidation peaks were observed at close potential values (E_{pa} = −1.15 and −1.05 V), indicating that the coordination sphere has been reorganized upon electron transfer in the time scale of the experiment (see Figure 5A). Exhaustive electrolysis of the complex solution was performed at E = −1.40 V; the voltammogram of the resulting system (Figure 5B) exhibited flat curves in the range −1.4 to 0 V, providing evidence for the demetalation of the chelate after reduction of Cu(II) into Cu(I). Such hypothesis was confirmed by the observation of Cu(0) sediment on the electrode surface after electrolysis. DFT calculations performed at the TPSSh/TZVP level on the $[Cu(te1th)]^+$ system provide a minimum

DOI: 10.1021/acs.inorgchem.5b01779
Inorg. Chem. XXXX, XXX, XXX−XXX

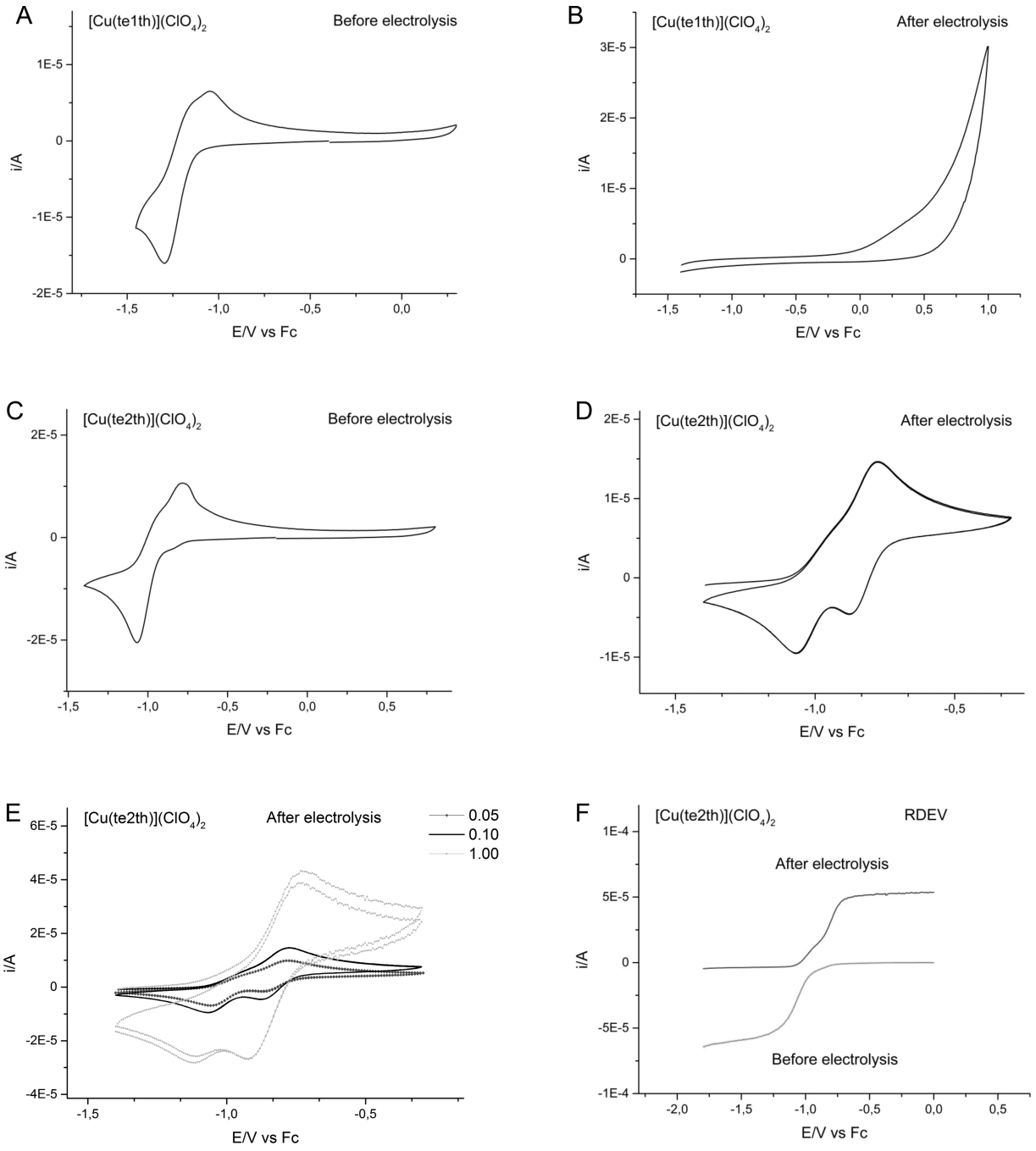

Figure 5. Cyclic voltammetry at a glassy carbon working electrode in CH_3CN/NBu_4PF_6 0.1 M (E/V vs Fc): complex [Cu(**te1th**)]$(ClO_4)_2$ (1.04 mM) (v = 0.1 V s^{-1}) before (A) and after (B) electrolysis at E = −1.40 V, and complex [Cu(**te2th**)]$(ClO_4)_2$ (1.07 mM) (v = 0.1 V s^{-1}) before (C) and after (D) electrolysis at E = −1.20 V. (E) CVs (2 cycles) of [Cu(**te2th**)]$(ClO_4)_2$ after electrolysis for v = 0.05 V s^{-1}, 0.1 V s^{-1}, 1 V/s with positive initial scan. (F) Rotating disk electrode voltammogram (1000 t min^{-1}) of [Cu(**te2th**)]$(ClO_4)_2$ before and after electrolysis.

energy conformation corresponding to a *trans*-I configuration, with the thiazole unit being coordinated through the nitrogen atom (Figure S21). All the remaining conformations explored (S-bonded *trans*-I, N-, and S-bonded *trans*-III and *cis*-V isomers) present considerably higher energies (7.0−33.8 kJ mol^{-1}, Table S2). These results suggest that the Cu(I) complex adopts a *trans*-I configuration in solution, although an exocyclic coordination of the metal ion cannot be ruled out.

The cyclic voltammograms of the $[Cu(\mathbf{te2th})]^{2+}$ complex reveal a slightly different redox behavior compared to $[Cu(\mathbf{te1th})]^{2+}$: reduction of the complex was detected at E_{pc} = −1.05 V, whereas oxidation occurred at E_{pa} = −0.94 and −0.78 V on the backscan (Figure 5C). Full electrolysis of the complex in solution was performed at E = −1.20 V in order to obtain the corresponding Cu(I) complex (n = $1e^-$). Rotating-disk electrode voltammetry (RDEV) after electrolysis showed two anodic waves at −1.04 and −0.81 V, the major system being oxidized at the highest potential (Figure 5F). This result, which is in strong contrast with that obtained for $[Cu(\mathbf{te1th})]^{2+}$, indicates that the Cu(I) complex does not disproportionate under these experimental conditions. Moreover, it shows that electron transfer has induced a significant

DOI: 10.1021/acs.inorgchem.5b01779
Inorg. Chem. XXXX, XXX, XXX−XXX

modification of the coordination sphere regarding the 230 mV positive shift of the main system (Figure 5D). In order to further investigate these results, CV experiments were performed at variable scan rate for 0.02 V s^{-1} < ν < 2 V s^{-1} with the electrolyzed solution. At a moderate scan rate (0.1 V s^{-1}), two quasi-reversible systems were detected at close potential values (E^0 = −0.99 and −0.82 V), the first oxidation peak being less well-defined (Figure 5D). Increase of the scan rate ν induced a significant modification on the cathodic part of the CV (Figure 5E). Hence, the ratio of the peak currents at E_{pc} = −0.87 and −1.05 V was strongly modified in favor of the peak at −0.87 V. These results are consistent with the formation, by electrochemical oxidation, of a transient Cu(II) species which is reduced at −0.87 V. This complex is in equilibrium with the thermodynamic Cu(II) species which can be reduced at −1.05 V.

In contrast with the results obtained for [Cu(**te1th**)]$^+$ (Figure S29), DFT calculations on [Cu(**te2th**)]$^+$ gave a minimum energy conformation with the cyclam unit presenting a *cis*-V configuration, the two pendant arms remaining uncoordinated (Figure 6). The optimized structure presents a

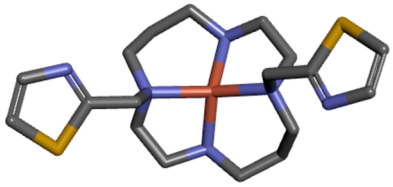

Figure 6. Optimized structure of [Cu(**te2th**)]$^+$ obtained with DFT calculations (TPSSh/TZVP).

nearly undistorted C_2 symmetry with two pairs of Cu−N distances of 2.06 Å and 2.12 Å, respectively. Very similar structures were observed in the solid state for a Cu(I) complex of 4,11-dimethyl-1,4,8,11-tetraazacyclotetradecane ligand functionalized with ferrocenyl groups,[37] and a Cu(I) complex of a cross-bridged cyclam derivative containing two benzyl pendant arms.[38] In the latter case the corresponding Cu(II) complex presented a similar structure with the metal coordination environment being completed by an acetonitrile ligand. Taking these precedents into account, the transient Cu(II) species reduced at −0.87 V is attributed to a *cis*-V isomer resulting from the oxidation of the most stable Cu(I) species, while the thermodynamically stable Cu(II) complex presents a *trans*-III structure (Figure 7).

Values (vs NHE) of reduction potential of Cu(II) complexes of **te1th**, **te2th**, and the other cyclam-based ligands H_4teta, H_2te2a, and H_2cb-te2a in aqueous solvents are gathered in Table 8. The E_{pc} values of Cu(II) complexes provide the following order of ligands according to their ability to stabilize Cu(I): **te2th** > **te1th** ∼ H_4teta > cb-te2a ∼ H_2te2a, the [Cu(**te2th**)]$^{2+}$ complex being the easiest one to be reduced. This is expected considering the softer nature of the donor atoms of the ligand (N and S) in comparison to the polyaminocarboxylates listed in Table 8. This complex exhibits a potential E_{pc} = −0.41 V (vs NHE) that is close to the threshold of −0.4 V for typical bioreductors, being slightly lower than that of NADH (E^0 = −0.32 V).[39] The quasi-reversibility of the redox system by cyclic voltammetry clearly shows that the chelate does not dissociate upon reduction of Cu(II) to Cu(I) within the time scale of the experiment (ca. 10 s, see Figure S28).

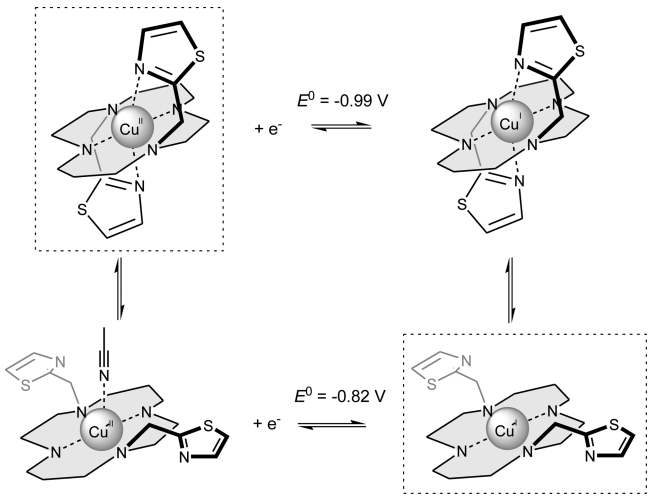

Figure 7. Electrochemistry behavior of the [Cu(**te2th**)] complex in acetonitrile according to analytical results (thermodynamically stable species are framed).

Table 8. Reduction Potentials (vs NHE) for the Copper(II) Complexes of te1th and te2th Ligands, and Similar Complexes from the Literature

	te1th	**te2th**	H_4teta[a]	H_2te2a[a]	H_2cb-te2a[b]
E_{pc}/V[c]	−0.65	−0.41	−0.6[d]	−0.9[d]	−0.86

[a]Ref 36b. [b]Ref 36a. [c]Experimental error = 5 mV. [d]Irreversible system.

CONCLUSIONS

The syntheses of two new cyclam derivatives mono-*N*- and di-N_1,N_8-functionalized by methylthiazolyl arms, respectively **te1th** and **te2th**, were achieved by using two different efficient selective-protection methods involving the preparation of phosphoryl cyclam or cyclam-bisaminal intermediates. The final compounds were obtained in only three steps with good overall yields, and their X-ray structures were determined and discussed. The copper(II) and zinc(II) complexes were synthesized, and the structures of [Cu(**te1th**)]$^{2+}$, [Cu(**te2th**)]$^{2+}$, and [Zn(**te2th**)]$^{2+}$ were determined by single-crystal X-ray diffraction, which revealed N5 or N6 coordination spheres for the complexes of **te1th** and **te2th**, respectively. The results reported in this paper also show that the combination of spectroscopic techniques such as EPR and NMR with DFT calculations represent a very powerful tool to establish the structures of metal complexes in solution.

The introduction of the methylthiazolyl groups does not influence significantly the basicity of the nitrogen atoms of the macrocycle compared to other mono-*N*- or di-N_1,N_8-functionalized cyclam compounds. Besides, the thermodynamic stability of the copper(II) complexes was found to be quite high, with a high selectivity for this metal ion over Zn^{2+} being observed in both cases. Another desirable property offered by these ligands is their very fast complexation of Cu^{2+} even in acidic solution. The [Cu(**te1th**)]$^{2+}$ complex was found to be very inert with respect to dissociation, while increasing the number of pendant arms provokes a faster dissociation of the [Cu(**te2th**)]$^{2+}$ complex in acidic media. Upon reduction to Cu(I), the complex of **te1th** was found to dissociate rather quickly in acetonitrile solution, while the **te2th** analogue is considerably more stable: this has to be underlined knowing the rare examples of stable Cu(I) cyclam based chelates reported in the

DOI: 10.1021/acs.inorgchem.5b01779
Inorg. Chem. XXXX, XXX, XXX−XXX

literature. Our results suggest that this is likely related to the difference in the structure of the two Cu(I) complexes. Finally, the results of our studies suggest that S-coordination of the thiazolyl groups to either Cu(I) or Cu(II) does not occur. Our ongoing work is dedicated to finding the adequate chelate design to provide such behavior: two options consisting of changing the size of the macrocyclic ring (using other polyazamacrocycles) to modulate the position of the metal center, or lengthening the arm (introducing ethylthiazolyl arms rather than methylthiazolyl) to facilitate a coordination inversion, may be envisaged. Additional efforts are also devoted to introduce additional hydrophilic groups to increase the solubility of such chelators in water when necessary. Anyway, when compared to other ligands reported in the literature including our own picolinate chelators, the thiazolyl ligands, especially **te2th**, offer quite good properties, especially in the kinetic and electrochemical inertness, while maintaining an equivalent thermodynamic stability and a copper(II) selectivity over zinc(II), suggesting promising results once the chelator design is improved.

EXPERIMENTAL SECTION

General Methods. Reagents used for the synthesis were purchased from Acros Organics and Sigma-Aldrich and used without further purification. The reagent cyclam was purchased from CheMatech (Dijon, France). Acetonitrile, toluene, and dichloromethane were distilled before use. Aluminum oxide (Sigma-Aldrich, activated, neutral, Brockmann I) was used for column chromatography. Precursors 2-bromomethyl-thiazole (**1**),[17] decahydro-3*H*-2a,5a,8,11a-tetraaza-2a^1-phosphacyclonona[*cd*]indene 2a^1-oxide (**2**),[18] and 1,4,8,11-tetraazatricyclo[9.3.1.1^{4,8}]hexadecane (**4**)[19] were synthesized according to the literature methods. The following instruments were used for the characterization. For NMR, ^{1}H, ^{31}P, and ^{13}C NMR spectra were recorded with Bruker Avance 500 (500 MHz for ^{1}H), Bruker Avance III HD 500 (500 MHz for ^{1}H), or Bruker DRX 300 (300 MHz for ^{1}H) spectrometers. For high-resolution mass spectrometry, a HRMS Q-Tof MaXis instrument was used, with sources ESI, APCI, APPI, nano-ESI (at the Institute of Organic and Analytic Chemistry, ICOA).

8-(Thiazol-2-ylmethyl)decahydro-3*H*-2a,5a,8,11a-tetraaza-2a1-phosphacyclonona[*cd*]indene-2a1-oxide (3). Phosphoryl cyclam **2** (0.749 g, 3.07 mmol) was dissolved in 15 mL of dry CH_3CN, and K_2CO_3 (1.413 g, 3.3 equiv, 10.22 mmol) was added. The mixture was cooled to 0 °C, and a solution of compound **1** (0.606 g, 1.1 equiv, 3.40 mmol) was added dropwise. The reaction was stirred at room temperature during 48 h. The suspension was filtered, and the solution was evaporated to dryness. The crude product was purified by column chromatography in aluminum oxide (using $CHCl_3$ as eluent) to yield the desired compound **3** as a pale yellow precipitate (0.886 g, 85%). ^{1}H NMR ($CDCl_3$, 298 K, 300 MHz): δ(ppm) = 7.54 (d, J = 3.2 Hz, 1 H, th), 7.13 (d, J = 3.1 Hz, 1 H, th), 3.88−3.55 (m, 4 H), 3.25−3.07 (m, 3 H), 3.06−2.32 (m, 11 H), 1.83−1.56 (m, 2 H, β-CH_2 cyclam), 1.54−1.29 (m, 2 H, β-CH_2 cyclam). ^{13}C NMR ($CDCl_3$, 295 K, 75.5 MHz): δ(ppm) = 170.73 (quaternary C, th), 141.86, 119.57 (tertiary C, th), 54.75, 53.02, 51.35, 51.07, 45.17 (d, $^2J_{C-P}$ = 15.4 Hz), 44.31 (d, $^2J_{C-P}$ = 11.0 Hz), 42.00, 41.73, 40.32 (d, $^2J_{C-P}$ = 3.4 Hz) (secondary C), 26.00 (secondary C, β-CH_2 cyclam), 21.81 (d, $^2J_{C-P}$ = 2.2 Hz) (secondary C, β-CH_2 cyclam). ^{31}P NMR ($CDCl_3$, 295 K, 121.5 MHz): δ(ppm) = 25.12. HRMS: m/z found 342.1514, calcd $C_{14}H_{25}N_5OPS^+$ (MH^+) 342.1512.

2-((1,4,8,11-Tetraazacyclotetradecan-1-yl)methyl)thiazole (te1th). A solution of compound **3** (0.052 g, 0.15 mmol) in 3 M HCl (10 mL) was stirred at room temperature for 12 h. The solution was concentrated, and the residue was purified on an ion-exchange resin (Dowex 1X2, 100−200 mesh) activated with Cl^-, to give 0.065 g of the desired compound as a yellow pale solid (**te1th**·5HCl, 89%). In order to get the neutral form of the ligand, **te1th**·5HCl was dissolved in distilled water, basified with 4 M NaOH until pH ∼12, and then extracted with $CHCl_3$ (3 × 30 mL). ^{1}H NMR ($CDCl_3$, 295 K, 300 MHz): δ(ppm) = 7.54 (d, J = 3.3 Hz, 1 H, th), 7.14 (d, J = 3.3 Hz, 1 H, th), 3.82 (s, 2 H, −CH_2− th), 2.74−2.44 (m, 20 H), 1.85−1.66 (m, 2 H, β-CH_2 cyclam), 1.58 (t, J = 5.4 and 5.4 Hz, 2 H, β-CH_2 cyclam). ^{13}C NMR ($CDCl_3$, 295 K, 75.5 MHz): δ(ppm) = 169.40 (quaternary C, th), 142.05, 119.35 (tertiary C, th), 77.59, 77.16, 76.73, 55.18, 54.40, 51.98, 50.70, 49.08, 48.60, 48.04, 47.66, 47.00, 43.51 (secondary C), 28.52, 26.09 (secondary C, β-CH_2 cyclam). HRMS: m/z 298.2060, calcd $C_{14}H_{28}N_5S^+$ (MH^+) 298.2060; m/z 149.6069 ([M + 2H]$^{2+}$), calcd $C_{14}H_{29}N_5S^{2+}$ 149.6066.

1,8-Bis(thiazol-2-ylmethyl)-1,4,8,11-tetraazatricyclo-[9.3.1.14,8]hexadecane-1,8-diium bromide (5). Cyclam bisformyl **4** (0.241 g, 1.07 mmol) was added to a solution of **1** (0.459 g, 2.4 equiv, 2.58 mmol) in 15 mL of freshly distilled acetonitrile. The mixture was heated to reflux during 4 days. The pale yellow precipitate was isolated by filtration, washed with acetonitrile, and dried under vacuum, to give 0.421 g of **5** (68%) as a white solid. ^{1}H NMR (D_2O, 295 K, 300 MHz): δ(ppm) = 7.88 (d, J = 3.4 Hz, 2H, th), 7.57 (d, J = 3.4 Hz, 2H, th), 4.16 (s, 4H, −CH_2− th), 3.34−2.85 (m, 16 H), 2.06−1.89 (m, 4H, β-CH_2 cyclam). ^{13}C NMR (D_2O, 295 K, 75.5 MHz): δ(ppm) = 144.67, 124.03 (tertiary C, th), 84.52 (secondary C, −CH_2− bisformyl), 57.93, 55.73, 50.72, 47.88 (secondary C); 25.60 (secondary C, β-CH_2 cyclam). HRMS (ESI$^+$): m/z 395.2048 ([M − formyl bridges + H])$^+$ calcd $C_{18}H_{31}N_6S_2^+$ 395.2046; m/z 198.1066 ([M − formyl bridges + 2H]$^{2+}$), calcd $C_{18}H_{32}N_6S_2^{2+}$ 198.1059.

1,8-Bis(thiazol-2-ylmethyl)-1,4,8,11-tetraazacyclotetradecane (te2th). Compound **5** (0.305 g, 0.53 mmol) was dissolved in 4 M NaOH (30 mL) and stirred during 12 h. The mixture was extracted with $CHCl_3$ (3 × 50 mL), and the combined organic extracts were dried on $MgSO_4$. The solvent was evaporated to give a yellow precipitate. The solid was dissolved in freshly distilled acetonitrile, and the insoluble impurities were filtered off, to give 0.533 g of **te2th** (84%) as a pale yellow solid. ^{1}H NMR ($CDCl_3$, 298 K, 300 MHz): δ(ppm) = 7.51 (d, 2 H, th), 7.08 (d, 2 H, th), 3.82 (s, 4 H, −CH_2− th), 2.59−2.43 (m, 16 H, α-CH_2 cyclam), 1.68−1.65 (m, 4 H, β-CH_2 cyclam). ^{13}C NMR ($CDCl_3$, 298 K, 75.5 MHz): δ(ppm) = 168.28 (quaternary C, th), 142.23, 119.25 (tertiary C, th), 54.26, 54.09, 50.18, 48.25, 47.21 (secondary C), 25.84 (secondary C, β-CH_2 cyclam). HRMS (ESI$^+$): m/z 395.2044 ([M + H]$^+$), calcd $C_{18}H_{31}N_6S_2^+$ 395.2046; m/z 198.1060 ([M + 2H]$^{2+}$), calcd $C_{18}H_{32}N_6S_2^{2+}$ 198.1059.

CAUTION! *Although no problem arose during our experiments, perchlorate salts and their metal complexes are potentially explosive and should be handled with great care and in small quantities.*[40]

[Cu(te1th)](ClO$_4$)$_2$. $Cu(ClO_4)_2·6H_2O$ (0.038 g, 0.9 equiv, 0.10 mmol) was added to a solution of **te1th**·5HCl (0.054 g, 0.11 mmol) in 2 mL of distilled water, and the mixture was stirred at room temperature during 48 h. After that, a small amount of K_2CO_3 was added to the mixture, which was stirred at room temperature during 3 days. The reaction mixture was concentrated to dryness. The impurities were precipitated by the addition of EtOH (5 mL) and filtered off. Concentration of the filtrate led to [Cu(**te1th**)]$(ClO_4)_2$ as a violet precipitate (0.056 g; 97%). HRMS (ESI$^+$): m/z 395.0964 ([M + (Cl)]$^+$) calcd $C_{14}H_{27}ClCuN_5S^+$ 395.0966; m/z 180.0639 ([M]$^{2+}$), calcd $C_{14}H_{27}CuN_5S^{2+}$ 180.0636.

[Zn(te1th)](ClO$_4$)$_2$. $Zn(ClO_4)_2·6H_2O$ (0.046 g, 1.0 equiv, 0.12 mmol) was added to a solution of **te1th**·5HCl (0.058 g, 0.12 mmol) in 5 mL of distilled H_2O. The pH was adjusted to 6 with NaOH, and the sample was then heated to reflux during 48 h. After that, the reaction mixture was allowed to cool to room temperature and then concentrated to dryness. The crude product was dissolved in 2 mL of MeOH and precipitated with Et_2O. The precipitate was isolated by filtration and dried under vacuum, to give 0.058 g of [Zn(**te1th**)]-$(ClO_4)_2$ (85%), as a white solid. ^{1}H NMR (D_2O, pD ∼6, 298 K, 500 MHz): δ(ppm) = 8.06 (d, 1 H, th), 7.95 (d, 1 H, th), 3.82 (s, 2 H, −CH_2− th), 2.68−2.45 (m, 16 H), 3.03−2.36 (m, 11 H), 1.77−1.69 (m, 2 H, β-CH_2 cyclam), 1.62−1.55 (m, 2 H, β-CH_2 cyclam). ^{13}C NMR (D_2O, pD ∼6, 298 K, 125.8 MHz): δ(ppm) = 175.18 (quaternary C, th), 141.52, 126.14, 125.95 (tertiary C, th), 63.45, 62.09, 60.02, 58.39, 57.55, 55.88, 55.13, 54.46, 53.95, 53.01, 52.78,

DOI: 10.1021/acs.inorgchem.5b01779
Inorg. Chem. XXXX, XXX, XXX−XXX

Table 9. Crystal Data and Refinement Details

	[Cu(**te1th**)](ClO$_4$)$_2$	[Cu(**te2th**)](ClO$_4$)$_2$	[Zn(**te2th**)](ClO$_4$)$_2$·H$_2$O
formula	$C_{14}H_{27}N_5Cl_2O_8SCu$	$C_{18}H_{30}N_6Cl_2O_8S_2Cu$	$C_{18}H_{32}N_6Cl_2O_9S_2Zn$
MW	559.91	657.04	676.91
crystal system	monoclinic	monoclinic	triclinic
space group	*C*2/*c*	*P*21/*n*	$P\bar{1}$
T [K]	298(2)	170(2)	170(2)
a [Å]	27.764(5)	9.5052(3)	9.7814(2)
b [Å]	12.9391(18)	14.0494(5)	16.8871(4)
c [Å]	14.198(2)	10.2388(4)	16.9644(4)
α [deg]	90	90	75.406(2)
β [deg]	115.07(2)	109.904(4)	79.394(2)
γ [deg]	90	90	89.335(2)
V [Å^3]	4620.0(12)	1285.64(8)	2663.65(10)
F(000)	2312	678	1400
Z	8	2	4
λ [Å] (Mo K*α*)	0.71073	0.71073	0.71073
D_{calc} [g cm^{-3}]	1.61	1.697	1.688
μ [mm^{-1}]	1.317	1.276	1.339
θ range [deg]	2.76−25.02	2.91−28.28	3.33−26.37
R_{int}	0.1602	0.0467	0.0895
reflns measd	15582	20403	38699
unique reflns	4077	3188	10862
reflns obsd	1401	2577	8204
GOF on F^2	0.845	1.019	1.05
*R*1[a]	0.0764	0.0289	0.046
*wR*2 (all data)[b]	0.1841	0.0729	0.1219
Largest ≠ peak and hole [e Å^{-3}]	0.724 and −0.367	0.44 and −0.253	0.703 and −0.569

[a] $R1 = \sum||F_o| - |F_c||/\sum|F_o|$. [b] $wR2 = \{\sum[w(|F_o|^2 - |F_c|^2)^2]/\sum[w(F_o^4)]\}^{1/2}$.

52.39, 52.13, 51.64, 51.23, 50.83, 50.14, 48.94, 48.15, 47.50 (secondary C), 29.98, 28.20, 27.67, 27.54, 26.50 (secondary C, *β*-CH_2 cyclam). HRMS (ESI$^+$): *m*/*z* 396.0962 ([M + (Cl)]$^+$), calcd $C_{14}H_{27}ClN_5SZn^+$ 396.0962; *m*/*z* 180.5638 ([M]$^{2+}$), calcd $C_{14}H_{27}N_5SZn^{2+}$ 180.5634.

[Cu(te2th)](ClO$_4$)$_2$. Cu(ClO$_4$)$_2$·6H$_2$O (0.094 g, 1.0 equiv, 0.25 mmol) was added to a solution of **te2th** (0.100 g, 0.25 mmol) in a solvent mixture containing 10 mL of CH_3CN and 2 mL of MeOH. The mixture was heated at 60 °C during 48 h, and then it was allowed to cool to room temperature and concentrated to dryness. The addition of MeOH (10 mL) resulted in the formation of a dark violet precipitate, which was isolated by filtration and dried under vacuum to give 0.148 g of [Cu(**te2th**)](ClO$_4$)$_2$ (89%). HRMS (ESI$^+$): *m*/*z* 556.0745 ([M + (ClO$_4$)]$^+$), calcd $C_{18}H_{30}ClCuN_6O_4S_2^+$ 556.0749; *m*/*z* 492.0949 ([M + (Cl)]$^+$) calcd $C_{18}H_{30}ClCuN_6S_2^+$ 492.0952; *m*/*z* 228.5633 ([M]$^{2+}$), calcd $C_{18}H_{30}CuN_6S_2^{2+}$ 228.5629.

[Zn(te2th)](ClO$_4$)$_2$. Zn(ClO$_4$)$_2$·6H$_2$O (0.075 g, 1.0 equiv, 0.20 mmol) was added to a solution of **te2th** (0.080 g, 0.20 mmol) in 10 mL of CH_3CN and 2 mL of MeOH, and the mixture was heated until reflux during 48 h. It was then allowed to cool to room temperature and concentrated to dryness. The product was precipitated by the addition of MeOH (10 mL), filtered off, and dried under vacuum to give 0.099 g of [Zn(**te2th**)](ClO$_4$)$_2$ (74%) as a white solid. ^{1}H NMR (CD_3CN, 298 K, 500 MHz): *δ*(ppm) = 7.98−7.96 (m), 7.85−7.82 (m), 7.68−7.61 (m), 4,72 (s), 4.66 (d, *J* = 18.7 Hz), 4.36 (d, *J* = 18.7 Hz), 4.26 (d, *J* = 19.7 Hz), 3.46−3.30 (m), 3.20−3.10 (m), 3.10−3.05 (m), 2.99−2.92 (m), 2.91−2.79 (m), 2.66−2.59 (m), 2.32−2.22 (m), 2.13−2.02 (m), 1.91−1.79 (m). ^{13}C NMR (CD_3CN, 298 K, 125.8 MHz): *δ*(ppm) = 172.48, 171.23 (quaternary C, th), 141.26, 139.82, 124.27, 124.16 (tertiary C, th), 61.89, 61.68, 60.50, 57.10, 56.00, 50.75, 49.81, 46.97, 46.22 (secondary C), 26.20, 25.95 (secondary C, *β*-CH_2 cyclam). HRMS (ESI$^+$): *m*/*z* 557.0742 ([M + (ClO$_4$)]$^+$), calcd $C_{18}H_{30}ClN_6O_4S_2Zn^+$ 557.0744; *m*/*z* 493.0947 ([M + (Cl)]$^+$), calcd $C_{18}H_{30}ClN_6S_2Zn^+$ 493.0948; *m*/*z* 229.0630 ([M]$^{2+}$), calcd $C_{18}H_{30}N_6S_2Zn^{2+}$ 229.0627.

EPR Spectroscopy. EPR spectra were recorded on a Bruker Elexsys 500 spectrometer operating at the X-band and equipped with a continuous-flow cryostat for liquid nitrogen. The EPR spectra of frozen aqueous solutions of the [Cu(**te1th**)]$^{2+}$ and [Cu(**te2th**)]$^{2+}$ complexes (at ca. 1 mM) containing 10% (v/v) of glycerol were recorded at 200 K at an attenuated microwave power of 0.2 mW and a microwave frequency (*ν*) of 9.31 GHz. The experimental EPR spectra were simulated in order to determine the relevant parameters (g_x, g_y, g_z, A_x, A_y, and A_z) using the SpinCount software.[30]

Single-Crystal X-ray Crystallography. Single-crystal X-ray diffraction data were collected with a Xcalibur 2 CCD 4-circle diffractometer (Oxford Diffraction) fitted with a graphite monochromated Mo K*α* radiation (*λ* = 0.71073 Å). Data were collected at 170 and 298 K. Crystal data and structure refinement details are given in Tables 9 and S1. Unit cell determination and data reduction, including interframe scaling, Lorentzian, polarization, empirical absorption, and detector sensitivity corrections, were carried out using attached programs of CrysAlis software (Oxford Diffraction).[41] Structures were solved by direct methods and refined by full matrix least-squares method on F^2 with the SHELXL97[42] suite of programs. The hydrogen atoms were identified at the last step and refined under geometrical restraints and isotropic U-constraints. CCDC 1411823, 1411824, 1411834, 1411834, and 1411836 contain the supplementary crystallographic data for this paper. These data can be obtained free of charge from The Cambridge Crystallographic Data Centre via www.ccdc.cam.ac.uk/data_request/cif. CIF files are also provided as Supporting Information.

Potentiometric Measurements. *Reagents and Solutions.* All solutions were prepared in ultrapure water. Carbonate-free solutions of the KOH titrant and HNO_3 titrant were prepared from a Fluka Analytical ampule diluted until 1 L with ultrapure water (freshly boiled for about 2 h and allowed to cool under argon). The titrant solutions were standardized using the Gran method.[43] The stock solutions of Cu^{2+} and Zn^{2+} were prepared from analytical grade salts and standardized by complexometric titrations with H_4edta (edta = ethylenediaminetetraacetic acid) following standards methods.[44]

Equipment and Working Conditions. Protonation and complexation titrations were performed in a 50 mL glass-jacketed titration cell

DOI: 10.1021/acs.inorgchem.5b01779
Inorg. Chem. XXXX, XXX, XXX−XXX

(Metrohm 727 TiStand), thermostatized at 25.0 ± 0.1 °C with a Lauda ecoline 003 circulating water bath and sealed from the atmosphere under nitrogen gas. The pH−potentiometric titrations were carried out by using a Metrohm 702 SM Titrino connected to a Metrohm 6.0234.100 combined glass electrode. A Metrohm Dosimat Plus autoburet (5 mL capacity) was used. Sample solutions for titrations contained approximately 0.05 mmol of **te1th** or 0.05 mmol for **te2th** in a total volume of 30 mL, except for the protonation of **te2th** were 0.02 mmol in 45 mL were used due to low solubility. The ionic strength was kept at 0.10 ± 0.01 M using KNO_3 as background electrolyte. In the complexation titrations, metal cations were added at 0.9 equiv of the ligand amount. In the case of Cu^{2+}, a competition with H_4edta in a batch titration in the intermediate pH range (3 to 9) was used, and a batch titration in the acid range (2−6) in the case of Zn^{2+}. Batch titrations were prepared in a similar way as the direct ones, but each titration point corresponded to 1/10 of the amount of the conventional one. Batch titration points were incubated in tightly closed vials at 25.0 ± 0.1 °C in a Lauda Alpha RA 24 thermostat during 4 weeks (until potential measurements reached complete stability). The titrations were automatically controlled by software upon selection of suitable parameters.

Measurements. The electromotive force of the sample solutions was measured after calibration of the electrode by titration of a standard 2×10^{-3} M HNO_3 solution. The $[H^+]$ of the samples was determined by the measurement of the electromotive force of the cell, $E = E^{\circ\prime} + Q \log [H^+] + E_j$, where the term pH is defined as $-\log [H^+]$. $E^{\circ\prime}$ and Q were determined by titration of a solution of known hydrogen-ion concentration at the same ionic strength. The liquid-junction potential, E_j, was found to be negligible under the experimental conditions used, and a value of $K_w = 10^{-13.78}$ was determined for our experimental conditions.

Calculation of Equilibrium Constants. Data from potentiometric titrations were used to determine the protonation constants of **te1th** and **te2th**, and the stability constants with the two metal ions. The overall equilibrium constants β_i^H and $\beta_{M_mH_hL_l}$ (being $\beta_{MmHhLl} = [M_mH_hL_l]/[M]^m[H]^h[L]^l$ and $\beta_{MH_{-1}L} = \beta_{ML(OH)} \times K_w$) were obtained by refinement of the potentiometric data with the HYPERQUAD program.[45] Differences, in log units, between the values of protonated (or hydrolyzed) and non-protonated constants provide the stepwise (log K) constants (being $K_{MmHhLl} = [M_mH_hL_l]/[M_mH_{h-1}L_l][H]$). The errors quoted are the standard deviations of the overall stability constants calculated by the program using all the experimental data. At least two titration curves for each system were fitted together. Species distribution diagrams were plotted from the calculated constants with the HYSS program.[46]

Electrochemistry. The electrochemical studies were performed in a glovebox (Jacomex) (O_2 < 1 ppm, H_2O < 1 ppm) with a home-designed three-electrode cell (WE, vitreous carbon; RE, Pt in Fc^+/Fc solution; CE, graphite rod). The potential of the cell was controlled by an Autolab PGSTAT 302 (Ecochemie) potentiostat monitored by a computer. The vitreous carbon electrode was carefully polished before each voltammetry experiment with a 1 μm alumina aqueous suspension and ultrasonically rinsed in water then acetone. Exhaustive electrolysis was performed with a graphite rod working electrode. The concentration in Cu complex was 10^{-3} M. An equimolar (1 mM) acetonitrile solution of ferrocene and ferrocenium hexafluorophosphate was used as internal reference. Ferrocene (Acros) was added to the electrolytic solution at the end of each series of experiments. All potential values were then recalculated against the ferrocene/ferrocenium couple. Acetonitrile (HPLC, VWR) was used as received and kept under argon in the glovebox after degassing. The supporting salt NBu_4PF_6 was synthesized from NBu_4OH (Fluka) and HPF_6 (Aldrich). It was then purified, dried under vacuum for 48 h at 100 °C, and kept under N_2 in the glovebox.

UV−Vis Spectrophotometry. The spectrophotometric measurements were performed in a Shimadzu UV spectrophotometer UV-1800 at 25 ± 0.1 °C, using quartz 1.0 cm cuvettes. The UV−vis spectrophotometric data were fitted using the HypSpec software.[47]

Formation and Dissociation Kinetic Studies. The rates of the Cu^{2+} complex formation with the **te1th** and **te2th** ligands were studied in buffered aqueous solutions at 25 °C by using a Shimadzu UV spectrophotometer (model UV-1800). Samples were measured in quartz cuvettes (optical path length = 1 cm), by following the increasing intensity of the complex d−d transition band in the visible range (~600 nm). Formation kinetic studies were carried out in acetate buffer at pH 3.8 and 5.6, at a constant ionic strength of 0.15 M. For these measurements, an equimolar amount of $CuCl_2$ stock solution was added to the stock solution of the **te1th** ligand ($[Cu^{2+}] = [$**te1th**$] = 1.1$ mM).

The acid-assisted dissociation kinetics of $[Cu($**te1th**$)]^{2+}$ and $[Cu($**te2th**$)]^{2+}$ complexes were followed under pseudo-first-order conditions in aqueous 5 M HCl solution at 30 and 50 °C, using a Unicam UV4 spectrophotometer. Concentrated acid was added to sample solutions containing the preformed complexes for an initial concentration of 3 mM, without control of ionic strength, and the decrease of the visible absorption bands of the complexes (538 nm for $[Cu($**te1th**$)]^{2+}$ and 550 nm for $[Cu($**te2th**$)]^{2+}$) was followed along time. The challenge tests with H_4edta were performed using an aqueous H_4edta solution buffered at pH 7.4 by adequate neutralization with KOH. The competitor solution was added to samples containing the preformed complexes for a final $edta^{4-}$ concentration of 200 mM and an initial complex concentration of 2 mM. The prepared samples were then kept at 37 °C in a thermostatic bath, and their spectra in the visible were measured each 24 h to follow the decrease of the absorption bands of the complexes.

Computational Details. Full geometry optimizations of the $[Cu($**te1th**$)]^{2+}$ and $[Cu($**te2th**$)]^{2+}$ systems were performed in aqueous solution employing unrestricted DFT calculations within the hybrid meta-GGA approximation with the TPSSh exchange-correlation functional[48] and the Gaussian 09 package (Revision D.01).[49] Similarly, the $[Cu($**te1th**$)]^{+}$, $[Cu($**te2th**$)]^{+}$, $[Zn($**te1th**$)]^{2+}$, and $[Zn($**te2th**$)]^{2+}$ complexes were fully optimized using the TPSSh functional and a restricted model. In these calculations we used the standard Ahlrichs' valence triple-ξ basis set including polarization functions (TZVP).[50] Solvent effects (water or acetonitrile) were included by using the polarizable continuum model (PCM), in which the solute cavity is built as an envelope of spheres centered on atoms or atomic groups with appropriate radii. In particular, we used the integral equation formalism (IEFPCM) variant as implemented in Gaussian 09.[51] No symmetry constraints have been imposed during the optimizations. The stationary points found on the potential energy surfaces as a result of geometry optimizations were tested to represent energy minima rather than saddle points via frequency analysis. Gibbs free energies were obtained at $T = 298.15$ K within the harmonic approximation. The default values for the integration grid (75 radial shells and 302 angular points) and the SCF energy convergence criteria (10^{-8}) were used in all calculations.

The calculations of the *g*- and *A*-tensors were carried out using the ORCA program package (Version 3.0.1)[52] and the methodology developed by Neese.[53] In these calculations we used the TPSS0 functional,[54] a 25% exchange version of TPSSh (10% exchange) that provides improved energetics.[55] The geometries of the complexes optimized with the Gaussian code as described above were employed for the calculation of *g*- and *A*-tensors. The center of the electronic charge was taken as the origin for the calculation of the *g*-tensor, which is a gauge dependent property. The different contributions to the *g*-tensor are the relativistic mass correction, the diamagnetic spin−orbit term, and the paramagnetic spin−orbit term. The *A*-tensor is calculated as a sum of three terms: (a) the isotropic Fermi contact (FC) term, (b) the spin-dipolar (SD) term, and (c) the spin−orbit coupling (SOC) term. The spin−orbit contributions to the hyperfine coupling constants and *g* values were computed via the spin−orbit mean field approach (SOMF) using the one-center approximation to the exchange term (SOMF(1X)).[56] The basis sets used for the EPR parameter calculations were the aug-cc-pVTZ-J basis set of Sauer for Cu,[57] and Ahlrichs's TZVP basis set for all other atoms.[50] The aug-cc-pVTZ-J basis set, which is described by a (25s17p10d3f2g)/[17s10p7d3f2g] contraction scheme, has been developed specifically

DOI: 10.1021/acs.inorgchem.5b01779
Inorg. Chem. XXXX, XXX, XXX−XXX

for the calculation of EPR parameters and includes four tight s-, one tight p-, and one tight d-type function to better describe the core region. The RIJCOSX approximation[58] was used to speed up calculations of the EPR parameters using the Def2-TZVPP/JK[59] auxiliary basis set as constructed automatically by ORCA. The convergence tolerances and integration accuracies of the calculations were increased from the defaults using the available TightSCF and Grid5 options. Solvent effects (water) were taking into account by using the COSMO solvation model as implemented in ORCA.[60]

The NMR shielding tensors of the $[Zn(\mathbf{te1th})]^{2+}$ and $[Zn(\mathbf{te2th})]^{2+}$ complexes were calculated in solution at the TPSSh/TZVP level using the GIAO method.[61] For ^{13}C NMR chemical shift calculation purposes the NMR shielding tensors of TMS were calculated at the same level. The calculated ^{13}C NMR chemical shifts were scaled using $\delta_{i,sca} = (\delta_{i,calc} - A)/B$, where $\delta_{i,calc}$ are the chemical shifts calculated with the GIAO method, and A and B are the intercept and the slope obtained from the linear correlations of plots of the experimental chemical shifts versus the calculated ones.[62]

■ ASSOCIATED CONTENT

Supporting Information

The Supporting Information is available free of charge on the ACS Publications website at DOI: 10.1021/acs.inorgchem.5b01779.

Figures S1−S29 and Tables S1−S4, giving ^1H, ^{13}C NMR, 2D NMR, MS, and HRMS of the compounds, ligands, and Zn complexes (at variable temperature and in variable solvents); X-ray structures of the ligands and relative crystallographic data; UV spectra of the complexation and dissociation studies; experimental X-ray data; DFT data and optimized geometries of the complexes (PDF)

X-ray crystallographic data for **te1th**·4HCl·3H_2O, **te2th**·4H_2O, $[Cu(\mathbf{te1th})]\cdot 2ClO_4$, $[Cu(\mathbf{te2th})]\cdot 2ClO_4$, and $[Zn(\mathbf{te2th})]\cdot 2ClO_4\cdot H_2O$(CIF)

■ AUTHOR INFORMATION

Corresponding Authors

*E-mail: delgado@itqb.unl.pt.
*E-mail: carlos.platas.iglesias@udc.es.
*E-mail: raphael.tripier@univ-brest.fr.

Notes

The authors declare no competing financial interest.

■ ACKNOWLEDGMENTS

R.T. acknowledges the Ministère de l'Enseignement Supérieur et de la Recherche, the Centre National de la Recherche Scientifique, and the "Conseil General du Finistère" for a postdoctoral fellowship for A.R.-R. R.T. also thanks the "Service Commun" of NMR and X-ray diffraction facilities of the University of Brest. C.P.-I. acknowledges Centro de Supercomputación de Galicia (CESGA) for providing the computer facilities. R.D. and L.M.P.L. acknowledge Fundação para a Ciência e a Tecnologia (FCT) for financial support under the Project PTDC/QEQ-SUP/2718/2012. L.M.P.L. thanks FCT also for a postdoctoral fellowship (SFRH/BPD/73361/2010).

■ REFERENCES

(1) Ametamey, S. M.; Honer, M.; Schubiger, P. A. *Chem. Rev.* **2008**, *108*, 1501−1516.
(2) Shokeen, M.; Anderson, C. J. *Acc. Chem. Res.* **2009**, *42*, 832−841.
(3) Ramogida, C. F.; Orvig, C. *Chem. Commun.* **2013**, *49*, 4720−4739.
(4) Price, E. W.; Orvig, C. *Chem. Soc. Rev.* **2014**, *43*, 260−290.
(5) (a) Bartholomä, M. D. *Inorg. Chim. Acta* **2012**, *389*, 36−51. (b) Wadas, T. J.; Wong, E. H.; Weisman, G. R.; Anderson, C. J. *Chem. Rev.* **2010**, *110*, 2858−2902.
(6) Di Bartolo, N.; Sargeson, A. M.; Donlevy, T. M.; Smith, S. V. *Dalton Trans.* **2001**, 2303−2309. Di Bartolo, N.; Sargeson, A. M.; Smith, S. V. *Org. Biomol. Chem.* **2006**, *4*, 3350−3357. Lears, K. A.; Ferdani, R.; Liang, K.; Zheleznyak, A.; Andrews, R.; Sherman, C. D.; Achilefu, S.; Anderson, C. J.; Rogers, B. E. *J. Nucl. Med.* **2011**, *52*, 470−477. Cooper, M. S.; Ma, M. T.; Sunassee, K.; Shaw, K. P.; Williams, J. D.; Paul, R. L.; Donnelly, P. S.; Blower, P. J. *Bioconjugate Chem.* **2012**, *23*, 1029−1039. Paterson, B. M.; Buncic, G.; McInnes, L. E.; Roselt, P.; Cullinane, C.; Binns, D. S.; Jeffery, C. M.; Price, R. I.; Hicks, R. J.; Donnelly, P. S. *Dalton Trans.* **2015**, *44*, 4901−4909.
(7) Juran, S.; Walther, M.; Stephan, H.; Bergmann, R.; Steinbach, J.; Kraus, W.; Emmerling, F.; Comba, P. *Bioconjugate Chem.* **2009**, *20*, 347−359. Comba, P.; Hunoldt, S.; Morgen, M.; Pietzsch, J.; Stephan, H.; Wadepohl, H. *Inorg. Chem.* **2013**, *52*, 8131−8143. Stephan, H.; Walther, M.; Fähnemann, S.; Ceroni, P.; Molloy, J. K.; Bergamini, G.; Heisig, F.; Müller, C. E.; Kraus, W.; Comba, P. *Chem. - Eur. J.* **2014**, *20*, 17011−17018.
(8) Wong, E. H.; Weisman, G. R.; Hill, D. C.; Reed, D. P.; Rogers, M. E.; Condon, J. P.; Fagan, M. A.; Calabrese, J. C.; Lam, K. C.; Guzei, I. A.; Rheingold, A. L. *J. Am. Chem. Soc.* **2000**, *122*, 10561−10572. Ferdani, R.; Stigers, D. J.; Fiamengo, A. L.; Wei, L.; Li, B. T. Y.; Golen, J. A.; Rheingold, A. L.; Weisman, G. R.; Wong, E. H.; Anderson, C. J. *Dalton Trans.* **2012**, *41*, 1938−1950. Comba, P.; Kubeil, M.; Pietzsch, J.; Rudolf, H.; Stephan, H.; Zarschler, K. *Inorg. Chem.* **2014**, *53*, 6698−6707.
(9) Bhattacharyya, S.; Dixit, M. *Dalton Trans.* **2011**, *40*, 6112−6128.
(10) Lima, L. M. P.; Esteban-Gómez, D.; Delgado, R.; Platas-Iglesias, C.; Tripier, R. *Inorg. Chem.* **2012**, *51*, 6916−6927. Frindel, M.; Camus, N.; Rauscher, A.; Bourgeois, M.; Alliot, C.; Barré, L.; Gestin, J.-F.; Tripier, R.; Faivre-Chauvet, A. *Nucl. Med. Biol.* **2014**, *41*, 49−57.
(11) Lima, L. M. P.; Halime, Z.; Marion, R.; Camus, N.; Delgado, R.; Platas-Iglesias, C.; Tripier, R. *Inorg. Chem.* **2014**, *53*, 5269−5279.
(12) Roger, M.; Lima, L. M. P.; Frindel, M.; Platas-Iglesias, C.; Gestin, J. F.; Delgado, R.; Patinec, V.; Tripier, R. *Inorg. Chem.* **2013**, *52*, 5246−5259.
(13) Woodin, K. S.; Heroux, K. J.; Boswell, C. A.; Wong, E. H.; Weisman, G. R.; Niu, W.; Tomellini, S. A.; Anderson, C. J.; Zakharov, L. N.; Rheingold, A. L. *Eur. J. Inorg. Chem.* **2005**, 4829−4833.
(14) Holland, J. P.; Barnard, P. J.; Collison, D.; Dilworth, J. R.; Edge, R.; Green, J. C.; McInnes, E. J. L. *Chem. - Eur. J.* **2008**, *14*, 5890−5907.
(15) Anderson, C. J.; Ferdani, R. *Cancer Biother. Radiopharm.* **2009**, *24*, 379−393.
(16) Bodio, E.; Boujtita, M.; Julienne, K.; Le Saec, P.; Gouin, S. G.; Hamon, J.; Renault, E.; Deniaud, D. *ChemPlusChem* **2014**, *79*, 1284−1293.
(17) Meier, H.; Nicklas, F.; Petermann, R. *Z. Z. Naturforsch.* **2007**, *62b*, 1525−1529.
(18) Filali, A.; Yaouanc, J. J.; Handel, H. *Angew. Chem., Int. Ed. Engl.* **1991**, *30*, 560−561.
(19) Royal, G.; Dahaoui-Gindrey, V.; Dahaoui, S.; Tabard, A.; Guilard, R.; Pullumbi, R.; Lecomte, C. *Eur. J. Org. Chem.* **1998**, 1971−1975.
(20) (a) Liang, X.; Weishäupl, M.; Parkinson, J. A.; Parsons, S.; McGregor, P. A.; Sadler, P. J. *Chem. - Eur. J.* **2003**, *9*, 4709−4717. (b) Liang, X.; Sadler, P. J. *Chem. Soc. Rev.* **2004**, *33*, 246−266. (c) Barefield, E. K. *Coord. Chem. Rev.* **2010**, *254*, 1607−1627.
(21) Bakaj, M.; Zimmer, M. *J. Mol. Struct.* **1999**, *508*, 59−72.
(22) (a) Yu, M.; Price, J. R.; Jensen, P.; Lovitt, C. J.; Shelper, T.; Duffy, S.; Windus, L. C.; Avery, V. M.; Rutledge, P. J.; Todd, M. H. *Inorg. Chem.* **2011**, *50*, 12823−12835. (b) El Majzoub, A.; Cadiou, C.; Dechamps-Olivier, I.; Tinant, B.; Chuburu, F. *Inorg. Chem.* **2011**, *50*, 4029−4038. (c) El Ghachtouli, S.; Cadiou, C.; Deshamps-Olivier, I.; Chuburu, F.; Aplincourt, M.; Roisnel, T. *Eur. J. Inorg. Chem.* **2006**, 3472−3481.
(23) Llunell, M.; Casanova, D.; Cirera, J.; Alemany, P.; Alvarez, S. *SHAPE, Program for the stereochemical analysis of molecular fragments by*

DOI: 10.1021/acs.inorgchem.5b01779
Inorg. Chem. XXXX, XXX, XXX−XXX

means of continuous shape measures and associated tools, Version 2.1; Barcelona, 2013.
(24) (a) Pinsky, M.; Avnir, D. *Inorg. Chem.* **1998**, *37*, 5575−5582. (b) Casanova, D.; Cirera, J.; Llunell, M.; Alemany, P.; Avnir, D.; Alvarez, S. *J. Am. Chem. Soc.* **2004**, *126*, 1755−1763. (c) Cirera, J.; Ruiz, E.; Alvarez, S. *Chem. - Eur. J.* **2006**, *12*, 3162−3167.
(25) (a) Choi, K.-Y.; Lee, H.-O.; Kim, Y.-S.; Chun, K.-M.; Lee, K.-C.; Choi, S.-N.; Hong, C.-P.; Kim, Y.-Y. *Inorg. Chem. Commun.* **2002**, *5*, 496−500. (b) Espinosa, E.; Meyer, M.; Berard, D.; Guilard, R. *Acta Crystallogr., Sect. C: Cryst. Struct. Commun.* **2002**, *58*, m119−m121. (c) Bucher, C.; Duval, E.; Barbe, J.-M.; Verpeaux, J.-N.; Amatore, C.; Guilard, R. *C. R. Acad. Sci., Ser. IIc: Chim.* **2000**, *3*, 211−222.
(26) (a) Tamanini, E.; Flavin, K.; Motevalli, M.; Piperno, S.; Gheber, L. A.; Todd, M. H.; Watkinson, M. *Inorg. Chem.* **2010**, *49*, 3789−3800. (b) Svobodova, I.; Havlickova, J.; Plutnar, J.; Lubal, P.; Kotek, J.; Hermann, P. *Eur. J. Inorg. Chem.* **2009**, 3577−3592.
(27) Lima, L. M. P.; Delgado, R.; Drew, M. G. B.; Brandão, P.; Félix, V. *Dalton Trans.* **2008**, 6593−6608.
(28) Rodríguez-Rodríguez, A.; Esteban-Gómez, D.; de Blas, A.; Rodríguez-Blas, T.; Fekete, M.; Botta, M.; Tripier, R.; Platas-Iglesias, C. *Inorg. Chem.* **2012**, *51*, 2509−2521.
(29) Regueiro-Figueroa, M.; Lima, L. M. P.; Blanco, V.; Esteban-Gómez, D.; de Blas, A.; Rodríguez-Blas, T.; Delgado, R.; Platas-Iglesias, C. *Inorg. Chem.* **2014**, *53*, 12859−12869.
(30) Simulations of EPR spectra were performed with the SpinCount software, created by Prof. M. P. Hendrich, at Carnegie Mellon University. SpinCount is available at http://www.chem.cmu.edu/groups/hendrich/.
(31) de Visser, S. P.; Quesne, M. G.; Martin, B.; Comba, P.; Ryde, U. *Chem. Commun.* **2014**, *50*, 262−282.
(32) Anderson, C. J.; Wadfas, T. J.; Wong, E. H.; Weisman, G. R. Q. *J. Nucl. Med. Mol. Imaging* **2008**, *52*, 185−192.
(33) Kotek, J.; Lubal, P.; Hermann, P.; Cisarova, I.; Lukes, I.; Godula, T.; Svobodova, I.; Taborsky, P.; Havel, J. *Chem. - Eur. J.* **2003**, *9*, 233−248.
(34) Paurova, M.; Havlickova, J.; Pospisilova, A.; Vetrik, M.; Cisarova, I.; Stephan, H.; Pietzsch, H.-J.; Hruby, M.; Hermann, P.; Kotek, J. *Chem. - Eur. J.* **2015**, *21*, 4671−4687.
(35) Šimeček, J.; Wester, H. J.; Notni, J. *Dalton Trans.* **2012**, *41*, 13803−13806.
(36) Pandya, D. N.; Kim, J. Y.; Park, J. C.; Lee, H.; Phapale, P. B.; Kwak, W.; Choi, T. H.; Cheon, G. J.; Yoon, Y.-R.; Yoo, J. *Chem. Commun.* **2010**, *46*, 3517−3519.
(37) Bucher, C.; Moutet, J.-C.; Pecaut, J.; Royal, G.; Saint-Aman, E.; Thomas, F. *Inorg. Chem.* **2004**, *43*, 3777−3779.
(38) Hubin, T. J.; Alcock, N. W.; Busch, D. H. *Acta Crystallogr., Sect. C: Cryst. Struct. Commun.* **2000**, *56*, 37−39.
(39) Schaetzle, O.; Barrière, F.; Baronian, K. *Energy Environ. Sci.* **2008**, *1*, 607−620.
(40) Wolsey, W. C. *J. Chem. Educ.* **1973**, *50*, A335−A337.
(41) (a) *CrysAlis CCD*, version 1.171.33.52; Oxford Diffraction Ltd.: Oxfordshire, UK, 2009. (b) *CrysAlis RED*, version 1.171.33.52; Oxford Diffraction Ltd.: Oxfordshire, UK, 2009.
(42) Sheldrick, G. M. *Acta Crystallogr., Sect. A: Found. Crystallogr.* **2008**, *64*, 112−122.
(43) Rossotti, F. J. C.; Rossotti, H. *J. Chem. Educ.* **1965**, *42*, 375−378.
(44) Schwarzenbach, G.; Flaschka, W. *Complexometric Titrations*; Methven & Co.: London, 1969.
(45) Gans, P.; Sabatini, A.; Vacca, A. *Talanta* **1996**, *43*, 1739−1753.
(46) Alderighi, L.; Gans, P.; Ienco, A.; Peters, D.; Sabatini, A.; Vacca, A. *Coord. Chem. Rev.* **1999**, *184*, 311−318.
(47) Gans, P.; Sabatini, A.; Vacca, A. *Ann. Chim.* **1999**, *89*, 45−49.
(48) Tao, J. M.; Perdew, J. P.; Staroverov, V. N.; Scuseria, G. E. *Phys. Rev. Lett.* **2003**, *91*, 146401.
(49) Frisch, M. J.; Trucks, G. W.; Schlegel, H. B.; Scuseria, G. E.; Robb, M. A.; Cheeseman, J. R.; Scalmani, G.; Barone, V.; Mennucci, B.; Petersson, G. A.; Nakatsuji, H.; Caricato, M.; Li, X.; Hratchian, H. P.; Izmaylov, A. F.; Bloino, J.; Zheng, G.; Sonnenberg, J. L.; Hada, M.; Ehara, M.; Toyota, K.; Fukuda, R.; Hasegawa, J.; Ishida, M.; Nakajima, T.; Honda, Y.; Kitao, O.; Nakai, H.; Vreven, T.; Montgomery, J. A., Jr.; Peralta, J. E.; Ogliaro, F.; Bearpark, M.; Heyd, J. J.; Brothers, E.; Kudin, K. N.; Staroverov, V. N.; Kobayashi, R.; Normand, J.; Raghavachari, K.; Rendell, A.; Burant, J. C.; Iyengar, S. S.; Tomasi, J.; Cossi, M.; Rega, N.; Millam, N. J.; Klene, M.; Knox, J. E.; Cross, J. B.; Bakken, V.; Adamo, C.; Jaramillo, J.; Gomperts, R.; Stratmann, R. E.; Yazyev, O.; Austin, A. J.; Cammi, R.; Pomelli, C.; Ochterski, J. W.; Martin, R. L.; Morokuma, K.; Zakrzewski, V. G.; Voth, G. A.; Salvador, P.; Dannenberg, J. J.; Dapprich, S.; Daniels, A. D.; Farkas, Ö.; Foresman, J. B.; Ortiz, J. V.; Cioslowski, J.; Fox, D. J. *Gaussian 09*, Revision A.01; Gaussian, Inc., Wallingford CT, 2009.
(50) (a) Schaefer, A.; Horn, H.; Ahlrichs, R. *J. Chem. Phys.* **1992**, *97*, 2571−2577. (b) Schaefer, A.; Huber, C.; Ahlrichs, R. *J. Chem. Phys.* **1994**, *100*, 5829−5835.
(51) Tomasi, J.; Mennucci, B.; Cammi, R. *Chem. Rev.* **2005**, *105*, 2999−3093.
(52) Neese, F. *Wiley Interdiscip. Rev.: Comput. Mol. Sci.* **2012**, *2*, 73−78.
(53) (a) Neese, F. *J. Chem. Phys.* **2003**, *118*, 3939−3948. (b) Neese, F. *J. Chem. Phys.* **2001**, *115*, 11080−11096. (c) Neese, F. *J. Phys. Chem. A* **2001**, *105*, 4290−4299.
(54) Grimme, S. *J. Phys. Chem. A* **2005**, *109*, 3067−3077.
(55) (a) Kesharwani, M. K.; Martin, J. M. L. *Theor. Chem. Acc.* **2014**, *133*, 1452. (b) Marzouk, A.; Madebène, B.; Alikhani, M. E. *J. Phys. Chem. A* **2013**, *117*, 4462−4471.
(56) Neese, F. *J. Chem. Phys.* **2005**, *122*, 34107.
(57) Hedegard, E. D.; Kongsted, J.; Sauer, S. P. A. *J. Chem. Theory Comput.* **2011**, *7*, 4077−4087.
(58) (a) Neese, F.; Wennmohs, F.; Hansen, A.; Becker, U. *Chem. Phys.* **2009**, *356*, 98−109. (b) Izsak, R.; Neese, F. *J. Chem. Phys.* **2011**, *135*, 144105. (c) Petrenko, T.; Kossmann, S.; Neese, F. *J. Chem. Phys.* **2011**, *134*, 54116. (d) Kossmann, S.; Neese, F. *Chem. Phys. Lett.* **2009**, *481*, 240−243.
(59) Weigend, F.; Ahlrichs, R. *Phys. Chem. Chem. Phys.* **2005**, *7*, 3297−3305.
(60) Sinnecker, S.; Rajendran, A.; Klamt, A.; Diedenhofen, M.; Neese, F. *J. Phys. Chem. A* **2006**, *110*, 2235−2245.
(61) Wolinski, K.; Hinton, J. F.; Pulay, P. *J. Am. Chem. Soc.* **1990**, *112*, 8251−8260.
(62) Mato-Iglesias, M.; Balogh, E.; Platas-Iglesias, C.; Toth, E.; de Blas, A.; Rodriguez-Blas, T. *Dalton Trans.* **2006**, 5404−5415.

DOI: 10.1021/acs.inorgchem.5b01779
Inorg. Chem. XXXX, XXX, XXX−XXX